The Pennsylvania State University
APPLIED RESEARCH LABORATORY
P.O. Box 30
State College, PA 16804

PROCESSING AND CHARACTERIZATION OF NIOBIUM ALUMINIDE-BASED COMPOSITES

by

S. A. Woytera
R. B. Bhagat

Technical Report No. TR 95-001
November 1995

Supported by:
Space and Naval Warfare Systems Command

L.R. Hettche, Director
Applied Research Laboratory

Approved for public release; distribution unlimited

REPORT DOCUMENTATION PAGE

Form Approved
OMB No. 0704-0188

1. AGENCY USE ONLY (Leave blank)	2. REPORT DATE	3. REPORT TYPE AND DATES COVERED
	November 1995	

4. TITLE AND SUBTITLE
PROCESSING AND CHARACTERIZATION OF NIOBIUM ALUMINIDE-BASED COMPOSITES

5. FUNDING NUMBERS

6. AUTHOR(S)
S. A. Woytera, R. B. Bhagat

7. PERFORMING ORGANIZATION NAME(S) AND ADDRESS(ES)
Applied Research Laboratory
The Pennsylvania State University
Post Office Box 30
State College, PA 16804

8. PERFORMING ORGANIZATION REPORT NUMBER
TR-95-01

9. SPONSORING / MONITORING AGENCY NAME(S) AND ADDRESS(ES)
Space and Naval Warfare Systems Command
2451 Crystal Drive
Arlington, VA 22245-5200

10. SPONSORING / MONITORING AGENCY REPORT NUMBER

11. SUPPLEMENTARY NOTES

12a. DISTRIBUTION / AVAILABILITY STATEMENT

12b. DISTRIBUTION CODE

13. ABSTRACT *(Maximum 200 words)*

Many ordered intermetallic compounds exhibit attractive properties for high temperature structural aerospace applications. These materials provide an alternative to and surpass the performance of existing high temperature superalloys and ceramics. High melting point, low density, high strength , and relatively good corrosion resistance are the attractive properties that have led to the current thrust of research in these materials. However, the major obstacles limiting the use of these materials are their low ductility and toughness at room temperature and poor creep resistance at elevated temperatures. Previous studies have shown that micro and macro-alloying of several systems lead to improvements in low temperature ductility and toughness, while the use of suitable ceramic reinforcements lead to increases in creep resistance. However, the reinforcements of the composites are not protected from reaction with the matrix at elevated temperatures. Thus, they do not have appropriate microstructures for thermal stability

Continued on next page.

14. SUBJECT TERMS
niobium, aluminide, composites, characterization
high temperature, ductibility, toughness, creep, ceramic

15. NUMBER OF PAGES
75

16. PRICE CODE

17. SECURITY CLASSIFICATION OF REPORT	18. SECURITY CLASSIFICATION OF THIS PAGE	19. SECURITY CLASSIFICATION OF ABSTRACT	20. LIMITATION OF ABSTRACT
UNCLASSIFIED	UNCLASSIFIED	UNCLASSIFIED	

and are likely to have poor creep resistance at elevated temperatures. In this investigation a novel approach has been devised to address both low and high temperature problems by the incorporation of "treated" refractory metal and ceramic reinforcements into a niobium aluminide matrix. The "treated" ductile phase is to improve room temperature toughness and the "treated" ceramic phase is to improve creep resistance. The "treatment", an oxide layer produced on the reinforcements (niobium and silicon carbide whiskers) by elevated temperature exposure, is to protect them from reacting with the matrix materials during hot pressing or subsequent use at elevated temperatures. A thermodynamic study using SOLGASMIX suggests that the "treated" reinforcements are likely to be protected from an adverse reaction with the matrix during the exothermic reaction between elemental niobium and aluminum powders and subsequently with the niobium aluminide matrix during processing. Thus the fabricated composites are expected to be thermally stable when exposed to elevated temperatures. Also, these composites are expected to have favorable characteristics of the interfaces for improved fracture toughness at room or low temperatures. Process optimization has led to the formation of Nb_3Al matrix, while reducing adverse reactions between the matrix and the reinforcements. The fabricated composites show relatively low hardness and higher toughness in comparison with the composites reinforced with the untreated whiskers.

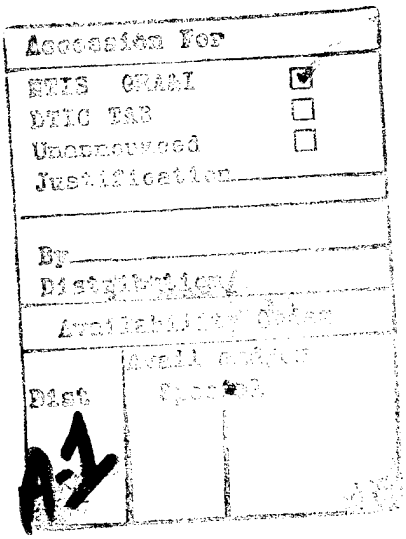

ABSTRACT

Many ordered intermetallic compounds exhibit attractive properties for high temperature structural aerospace applications. These materials provide an alternative to and surpass the performance of existing high temperature superalloys and ceramics. High melting point, low density, high strength, and relatively good corrosion resistance are the attractive properties that have led to the current thrust of research in these materials. However, the major obstacles limiting the use of these materials are their low ductility and toughness at room temperature and poor creep resistance at elevated temperatures. Previous studies have shown that micro and macro-alloying of several systems lead to improvements in low temperature ductility and toughness, while the use of suitable ceramic reinforcements lead to increases in creep resistance. However, the reinforcements of the composites are not protected from reaction with the matrix at elevated temperatures. Thus, they do not have appropriate microstructures for thermal stability and are likely to have poor creep resistance at elevated temperatures. In this investigation a novel approach has been devised to address both low and high temperature problems by the incorporation of "treated" refractory metal and ceramic reinforcements into a niobium aluminide matrix. The "treated" ductile phase is to improve room temperature toughness and the "treated" ceramic phase is to improve creep resistance. The "treatment", an oxide layer produced on the reinforcements (niobium and silicon carbide whiskers) by elevated temperature exposure, is to protect them from reacting with the matrix materials during hot pressing or subsequent use at elevated temperatures. A thermodynamic study using SOLGASMIX suggests that the "treated" reinforcements are likely to be protected from an adverse reaction with the matrix during the exothermic reaction between elemental niobium and aluminum powders and subsequently with the niobium aluminide matrix during processing. Thus the fabricated composites are expected to be thermally stable when exposed to elevated

temperatures. Also, these composites are expected to have favorable characteristics of the interfaces for improved fracture toughness at room or low temperatures. Process optimization has led to the formation of Nb_3Al matrix, while reducing adverse reactions between the matrix and the reinforcements. The fabricated composites show relatively low hardness and higher toughness in comparison with the composites reinforced with the untreated whiskers.

TABLE OF CONTENTS

List of Figures

List of Tables

Chapter 1

INTRODUCTION

Many ordered intermetallic compounds exhibit attractive properties for high temperature structural aerospace applications. These materials provide an alternative to and surpass the performance of existing high temperature superalloys and ceramics. High melting point, low density, high strength, and relatively good corrosion resistance are the attractive properties that have led to the current thrust of research in these materials. However, the major obstacles limiting the use of these materials are their low ductility and toughness at room temperature and poor creep resistance at elevated temperatures.

1.1 Background

An intermetallic is generally an ordered phase that exists in a relatively narrow composition range between two metallic elements.

Ordered Structure:

In an alloy composed of A and B atoms, the atoms can be arranged in one of two ways, ordered or disordered as shown below.

Ordered	Disordered
A B A B A B	A A B A B B
B A B A B A	A B B B A A
A B A B A B	B A B B A B

For an ordered structure to exist the attraction between different (A and B) atoms must be greater than the attraction between like (A-A or B-B) atoms [1]. The energy between the A-B atom must be greater than one half the energy of the A-A atoms plus that of the B-B atoms. Most intermetallic compounds exist as one of five different stoichiometric combinations between the A and B elements (A_3B, A_2B, A_5B_3, A_7B_6 , and AB).

Order in intermetallics can be termed as either long or short-range. Large distances of order at lower temperature constitutes long range order. As temperature increases long range order decreases, i.e. entropy increases until a critical temperature (T_c) is reached. Long-range order is destroyed at T_c, though at temperatures above T_c small regions of order exist. These regions are called regions of short-range order. States of disorder could be retained if a material were quenched from temperatures above T_c. Order could then be restored by annealing (Fig 1.1).

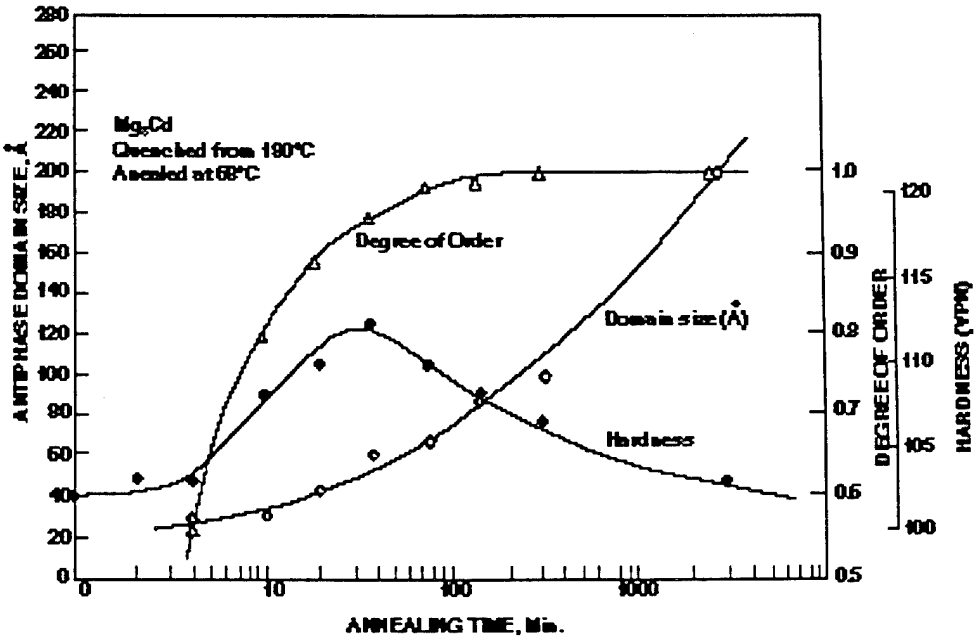

Figure 1.1. Effect of annealing time on long-range order [2].

Single dislocation motion in an ordered alloy will destroy the order and produce undesirable atomic bonding across the slip plane as shown in Fig. 1.2 a and 1.2b [3]. Very high energy (stress) is needed for movement of a single dislocation due to the strong attraction between unlike atoms. Therefore, deformations which cause slip in ordered alloys travel in pairs. As the first dislocation passes and causes disorder a second dislocation follows and restores it (Fig. 1.2 c and 1.2d).

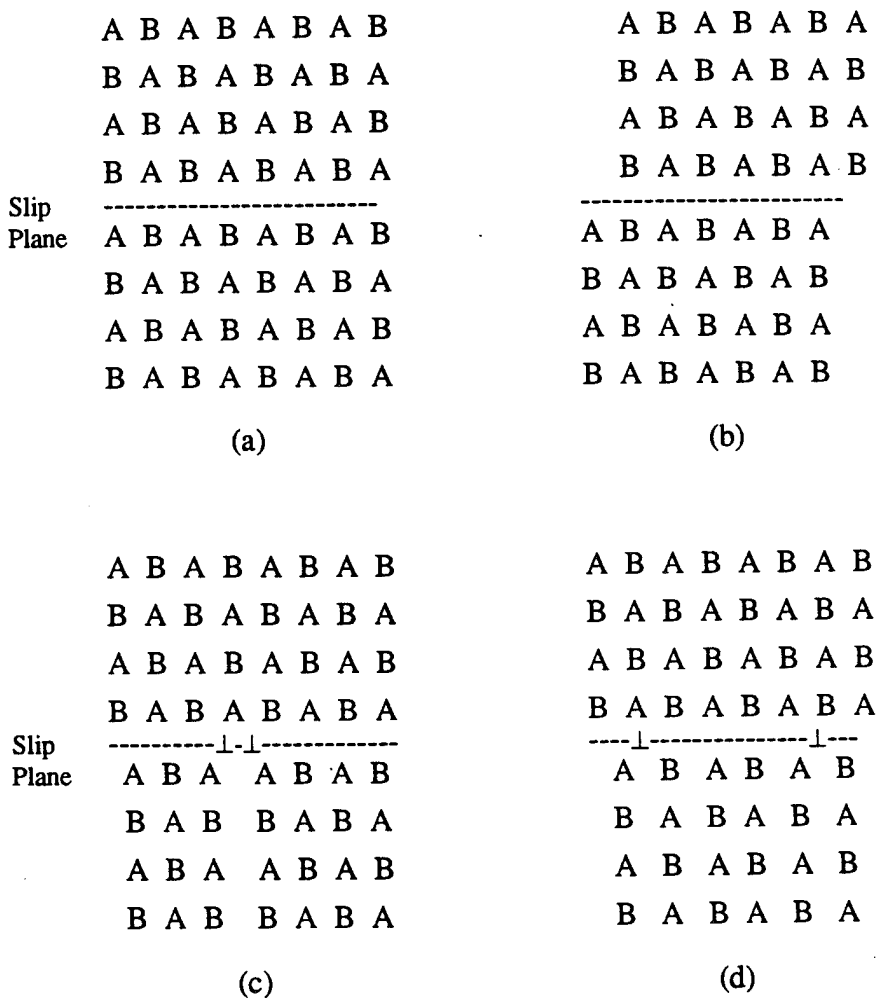

Fig. 1.2. (a) An ordered AB structure (b) Slip along plane producing undesirable neighbors. (c) Superlative dislocation motion, undesirable bonding not produced. (d) Supperlattice dislocation separation, undesirable bonding between dislocations [3].

These are called double or superlattice dislocations. It is evident from the nature of an ordered structure that cross-slip would be extremely difficult, and would lead to high work hardening rates.

Ordering increases the melting temperature of the alloy by increasing the energy required to change the atoms from one configuration to another. Looking at the binary phase diagram between Nb and Al (Fig 1.3) [4], it can be seen that the compounds of Nb_3Al, Nb_2Al, and $NbAl_3$ exhibit high melting temperatures. It could be assumed from their high melting temperature that these compounds have an ordered structure and are therefore intermetallics. Ordering can also affect the electrical resistivity and magnetic properties of an alloy as well as its strength. The strong attractive bonding between unlike neighbors in an ordered structure increases the materials strength. A plot of yield strength vs. T/T_m for several materials shows that ordered structures exhibit high strength at higher temperatures (Fig 1.4).

The high strength and high melting temperature of intermetallics does not come without a price, namely ductility and toughness. They have little or no ductility at room temperature, which renders them inappropriate for many structural applications. The major causes of brittleness in intermetallic compounds include: lack of enough slip systems (bulk brittleness), low mobility of superdislocations, and grain boundary weakness [5,6]. Deformation along slip planes becomes more complicated in intermetallics than in most metals due to the stronger bonding and closer packing of atoms. They are brittle like ceramics at low temperature but go through a brittle to ductile transition temperature at or above their use temperature where they exhibit metal-like properties.

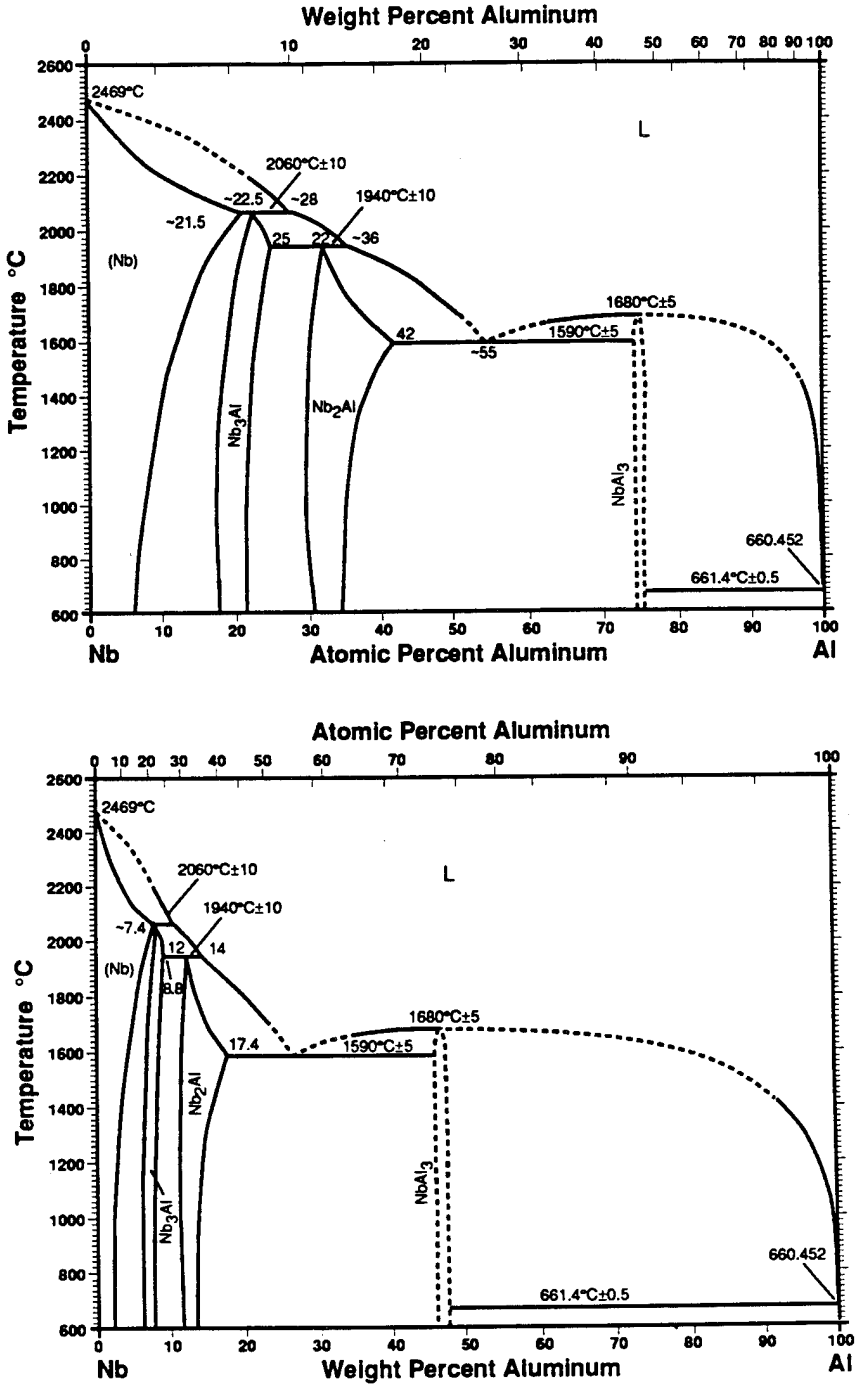

Figure 1.3 Nb-Al binary phase diagram (after Kattner, Ref. 4).

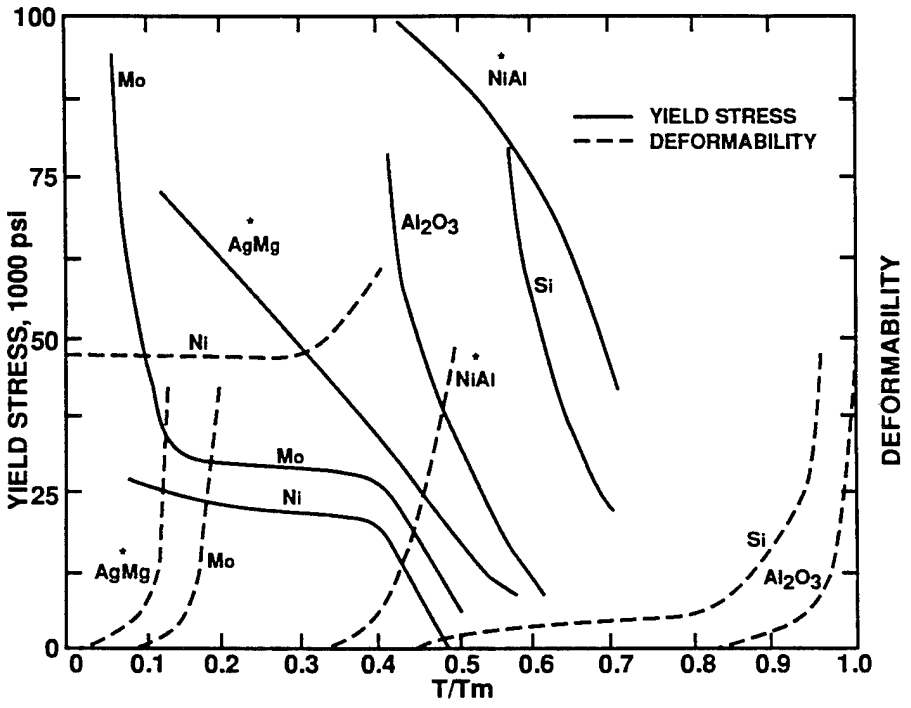

Figure 1.4 Yield strength vs. T/T_m for several materials [2].

It has been found that for extensive plasticity in polycrystals, at least five independent slip systems are needed [5,6]. Intermetallics usually have less than five as in the cubic B2 NiAl compound which exhibits only three independent systems or in the hexagonal Ti_3Al compound which has only two slip systems, contributing to its brittleness [6].

The cause of brittleness in intermetallics may also lie at the grain boundary due to the segregation of impurities there. A common case is hydrogen embrittlement. Co_3Ti is brittle in hydrogen but exhibits an elongation of 44 % in its absence. Even if impurities

are not present, brittleness can still be related to the grain boundary. Poor grain boundary cohesion strength is found in ordered alloys and related to the valency difference between the metal atoms [5]. An increasing valency difference increases grain boundary fracture.

1.2 Objective

The overall objective of this study is to improve both the room temperature ductility and toughness, and the high temperature strength and creep resistance of discontinuously reinforced niobium aluminide matrix composites. This thesis deals with the fabrication and room temperature properties of the composites. Our approach is to provide suitable coatings for selected reinforcements, followed by reaction hot pressing in vacuum. Nb_3Al has been selected as the matrix because of its attractive high temperature properties [7]. It exists over a narrow composition range (Fig. 1.3) and has a melting point of 2333 K [4]. This material, like many other intermetallics, has limited ductility owing to its low symmetry, complex crystal structure. Two different types of "treated" discontinuous reinforcements are incorporated into the matrix. The selected reinforcements are silicon carbide whiskers and niobium particles. The "treatments" are aimed at (a) providing protective coating for the reinforcements, thereby avoiding undesirable reactions with the intermetallic matrix and (b) tailoring the interfaces in the composite. The whisker reinforcement is to improve the high temperature strength and creep resistance. The room temperature ductility and toughness are expected to be improved by niobium particles providing ductile phase toughening. An oxide coating has been selected, due to its chemical stability and the relative ease of obtaining it by high temperature exposure of the reinforcements to air. A uniform coating is desired on the reinforcements to provide adequate protection from reaction with the matrix. A thermodynamic study using SOLGASMIX suggests that the "treated" reinforcements are

likely to be protected from an adverse reaction with the matrix during the exothermic reaction between elemental niobium and aluminum powders and subsequently with the niobium aluminide matrix during processing. Thus the fabricated composites are expected to be thermally stable when exposed to elevated temperatures. Also, these composites are expected to have favorable characteristics of the interfaces for improved fracture toughness at room or low temperatures.

Chapter 2

LITERATURE REVIEW

2.1 Improvements in Intermetallic Matrix Properties

Intermetallics such as aluminides and silicides are currently being considered for use in a wide variety of high temperature structural aerospace applications [6,8-14] because of their high melting point, relatively high strength, and low density. The intermetallics typically have an ordered structure and lack ductility and toughness at room temperature. Thus, the use of these materials will largely depend upon improving certain properties such as low temperature ductility, high-temperature strength and creep resistance [6,8-12]. Ductility and toughness of intermetallics at low temperatures have been improved in some systems such as Ni_3Al and Ti_3Al by microalloying [6,15-21] and macroalloying [15,16,22]. The creep resistance and toughness in intermetallics have been improved by the use of suitable reinforcements [23-25].

2.1.1 Microalloying

Microalloying is the addition of minor concentrations (< 1at.%) of elements to control grain boundary composition [16]. Microalloying has been proven in many studies to be an effective means to combat brittleness; additions of boron, carbon and beryllium have been found most effective in Ni_3Al and other $L1_2$ intermetallics [17,18]. Small additions of boron to Ni_3Al have been shown to increase its room-temperature elongation by 50% and change the fracture mode from solely intergranular to a mixture of intergranular and transgranular fracture [19,20]. Earlier studies have shown that the

grain boundary brittleness in Ni_3Al was the result of poor grain boundary cohesion and segregation of impurities at the boundaries. Boron was attributed to increase the grain boundary cohesion strength, thereby improving the ductility [16]. Recent investigations, however, have shown that boron reduces environmental embrittlement by reducing the diffusivity of hydrogen along the grain boundaries due to the strong segregation of boron to these boundaries [21]. This reduction in embrittlement results in increased toughness.

2.1.2 Macroalloying

Macroalloying has been used to change the crystal structure from one of low symmetry (hexagonal) to one of higher symmetry (such as an ordered cubic structure) in intermetallics. This promotes the activation of additional slip systems and can improve ductility [16]. Low symmetry crystal structures have a limited number of deformation modes, which leads to bulk brittleness in many intermetallics [15]. Higher symmetry structures, such as cubic, show increased ductility over hexagonal ordered alloys. The crystal structure of Co_3V was changed from a brittle hexagonal structure to a higher symmetry cubic structure by macroalloying with iron [22]. Room temperature elongations of greater than 40% were observed in the modified structure. Another system which shows increased room temperature ductility through macroalloying is Ti_3Al. Niobium additions increase the non-basal slip activity in the titanium aluminide thereby increasing the number of slip planes [26,27]. For this reason niobium is considered as the preferred beta phase stabilizer.

2.1.3 Reinforcement Additions

Reinforcements can be used to improve the fracture toughness by providing a relatively weak interface that will lead to crack blunting and fiber pull-out. Three features of the strengthening mechanisms have been reported by Vedula [28] for intermetallic composites: (a) brittle second phase additions such as silicon carbide whiskers will increase the energy of crack propagation at low temperature by producing an interface for crack deflection, (b) ductile second phase additions such as niobium and tantalum will delay crack propagation at low temperatures by absorbing energy through plastic deformation at the crack tip, and (c) at elevated temperatures a ceramic second phase (for example SiC or Al_2O_3) will provide improved creep resistance by inhibiting dislocation motion or grain boundary sliding. With relatively weak interfacial bonding the incorporation of high strength brittle reinforcements into a brittle matrix provides an alternate path for cracks to deflect, instead of continuing to grow across the matrix until a critical size is reached. Studies have shown improvements in both room temperature ductility and high temperature creep resistance of $MoSi_2$ when reinforced with SiC whiskers (20 vol.%); room temperature fracture toughness increased from 5.32 MPa$\sqrt{m}$ for the unreinforced material to 8.20 MPa$\sqrt{m}$ for the reinforced material produced by hot pressing [23,24]. Crack deflection has been observed as one of the toughening mechanisms [29]. Other possible mechanisms may include crack bowing, branching, bridging, and microcracking. Mendiratta et al. [25] have reported a fracture toughness of approximately 21 MPa$\sqrt{m}$ for the Nb / Nb_5Si_3 composite system. The composite was fabricated by arc casting which was followed by thermomechanical treatments. In comparison, monolithic Nb_5Si_3 has a fracture toughness between 1 and 2 MPa$\sqrt{m}$, as reported in Ref. 25. Another system, $MoSi_2$ reinforced with 20 vol.% of niobium particles or niobium laminates also has shown improved toughness [30,31]. Ductile phase toughening is accomplished by ductile bridging of intact ligaments behind the

crack tip i.e. ductile reinforcements help to blunt and retard crack propagation [32]. However, the reinforcements of the composites are not protected from reaction with the matrix at elevated temperatures. Thus, these composites do not have appropriate microstructures for thermal stability and are likely to have poor creep resistance at elevated temperatures. There is a need for tailoring the microstructure of the intermetallic matrix composites to prevent adverse reactions during the processing and also to alleviate the problem of the coefficient of thermal expansion (CTE) mismatch between the matrix and the reinforcement. Differences in thermal expansion coefficients of the intermetallic matrices and the fiber reinforcements (see Table 2.1) result in high residual stresses in the composites upon cooling from the processing temperature or during thermal cycling which could lead to microcracking and consequently poor mechanical properties.

Table 2.1. Properties of selected fiber reinforcements and aluminide matrix materials.

Material	CTE (ppm/K)	UTS (MPa)	Young's Modulus (GPa)
Reinforcement			
SiC (SCS-6)	5.1	4000	400
SiC (Nicalon)	3.1	2480-3240	179-207
SiC (HPZ)	---	2410-3100	152-193
Al_2O_3 (Saphikon)	8.3-9.0	2250	351
FP Al_2O_3	8	1400	380
Saffil ($96Al_2O_3+4SiO_2$)	8	2000	300
PRD-166 ($Al_2O_3+20ZrO_2$)	9	2100	380
3M Alumina (99% Al_2O_3)	8	2240-2760	379
Matrix			
NiAl	16	380	234
Ni_3Al (Ni-24Al-1.2Ti-.07Zr-.46B)	12.5	--	178
Ni_3Al (Ni-24Al-.7Y-.07Zr-1B)	12.5	--	178
IC-218 (Ni-16.3Al-7.8Cr-2Ti-.45Zr-.1B)	12.5	--	178
Ti_3Al+Nb	10	1100-1180	--
TiAl (Ti-48.4Al-1Mn)	10	---	176
FeAl	21	--	255
Fe_3Al (Fe-28Al-2Cr-1Ti)	16.5	--	141
$NbAl_3$	11	--	--

Chapter 3

THERMODYNAMIC ANALYSIS

3.1 SOLGASMIX

A thermodynamic study was performed using SOLGASMIX [33,34], a computer program to determine the chemical stability of the coated and uncoated reinforcements in the intermetallic matrix. SOLGASMIX contains thermochemical data for many compounds as listed in JANAF tables [35] and it is used to predict equilibrium states in chemical systems through the minimization of free energy. At times, additional thermochemical data for compounds not available in the existing database are needed. Data for expected compounds not present in the JANAF tables were included into the database (see Appendix A, Table A3.1).

3.2 Material Systems

Three different systems were investigated using SOLGASMIX as listed in Table 3.1. Experimental work was only performed for the niobium-aluminide system. Results for this system will be discussed in detail below, whereas SOLGASMIX results for the second and third systems will be presented in tabular form in Appendix A (Tables A3.2 - A3.5).

Table 3.1. Three material systems investigated by SOLGASMIX.

System #	Materials
1	$Nb + Al + SiC_w$
2	$Nb + Si + SiC_w$
3	$Mo + Si + SiC_w$

The three cases investigated for the fabrication of niobium-aluminide based composites are shown in Table 3.2.

Table 3.2. Three cases investigated using SOLGASMIX for the niobium aluminide system, the materials in brackets refer to the reinforcements with an appropriate oxide coating.

Case #	Materials
1	$Nb + Al + SiC_W$
2	$Nb + Al + [SiC_W]SiO_2$
3	$Nb + Al + [SiC_W]SiO_2 + [Nb]NbO_2$

The first case consists of the elemental matrix powders and the uncoated silicon carbide whiskers. The second case consists of the matrix powders and oxide coated silicon carbide whiskers. The third case consists of the matrix powders, the coated whiskers, and the coated niobium particles. The coatings for the reinforcements are the natural oxides, SiO_2 and NbO_2, that form on the surface of the silicon carbide whiskers and the niobium particles, respectively, during high temperature exposure to air.

Niobium and aluminum are input into SOLGASMIX in elemental form and silicon carbide is entered as a compound. The silicon carbide entered into SOLGASMIX does not take into account the structure or the size and shape of the material; therefore, the predicted reactions may not be completely realized in practice. Also, SOLGASMIX predictions are at equilibrium, when the reaction no longer proceeds in the forward or reverse direction. The reactions may not, however, reach equilibrium under the

experimental conditions. Thus, SOLGASMIX predictions do not tell us exactly what will happen experimentally, but they provide valuable guidelines for possible reactions and reaction products.

Predictions for case 1 (see Appendix A, Table A3.6) show that silicon carbide readily dissociates into silicon and carbon which in turn react with niobium to form niobium carbides and silicides under hot pressing conditions. Elemental silicon is also expected to combine with aluminum to form a solid solution. In case 2, silicon carbide is protected with a SiO_2 coating which reacts with aluminum and niobium to form niobium silicides and alumina (see Appendix A, Table A3.7). Protection of silicon carbide whiskers from reaction with niobium and aluminum will, of course, depend on the amount and uniformity of the coating layer. Case 3, which incorporates oxide coated silicon carbide whiskers and niobium particles shows enhanced chemical stability of the reinforcements with the aluminide matrix (see Appendix A, Table A3.8). Interfacial reaction products consist of NbO, SiO_2, Al_2O_3, NbO_2 or Nb_5Si_3.

Chapter 4

EXPERIMENTAL WORK

4.1 Materials

High purity (99.8%) Nb powder from Atlantic Equipment Engineers (AEE) was used. The median particle size was determined by a Horiba LA-900 particle size distribution analyzer to be 10.6 μm (Fig. 4.1). Al powder measured in the same way (from ALCOA) had a mean particle size of 6.4 μm (Fig. 4.2). The SiC whiskers, used for reinforcement, were purchased from Advanced Refractory Technologies (ART). The whiskers are M grade and have the following diameter and aspect ratio range, respectively: 0.7 - 1.2 μm, 10 - 25.

4.2 Treatment of Reinforcements

4.2.1 Reactor Design

A reactor had to be developed to produce the oxide coatings on the SiC whiskers and Nb particles. The operating range for both temperature and time for the production of an oxide layer on SiC whiskers and Nb particles had to be determined before a reactor could be designed and built. This was accomplished by placing small amounts of SiC whiskers in a ceramic crucible and heating them to specific temperatures for specific times. A temperature range near 1073 K was the starting point based on information

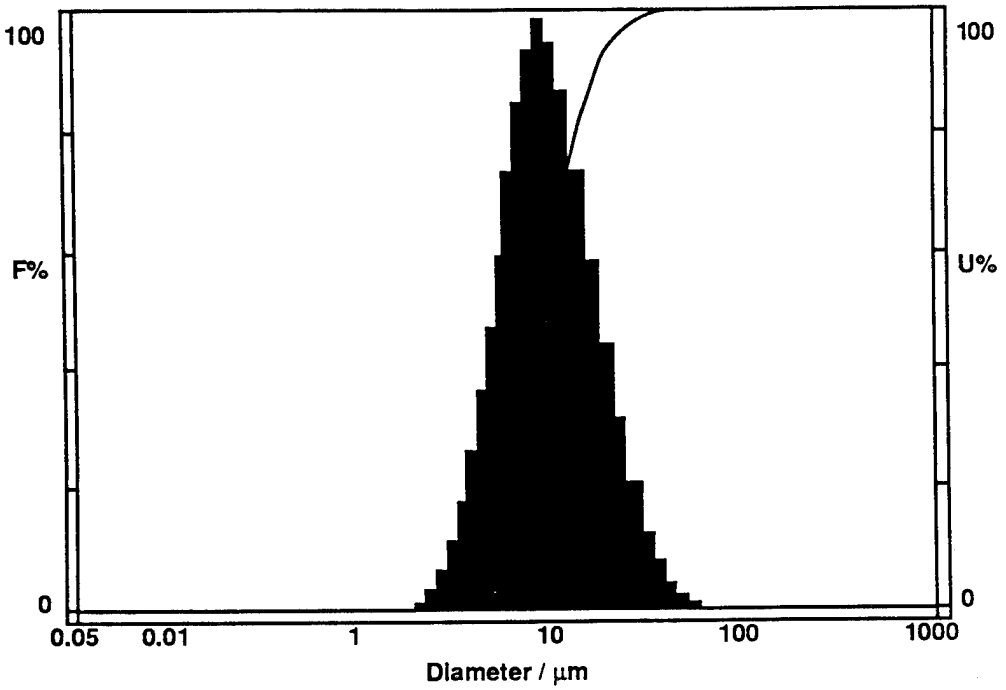

Figure 4.1 Nb powder particle size distribution.

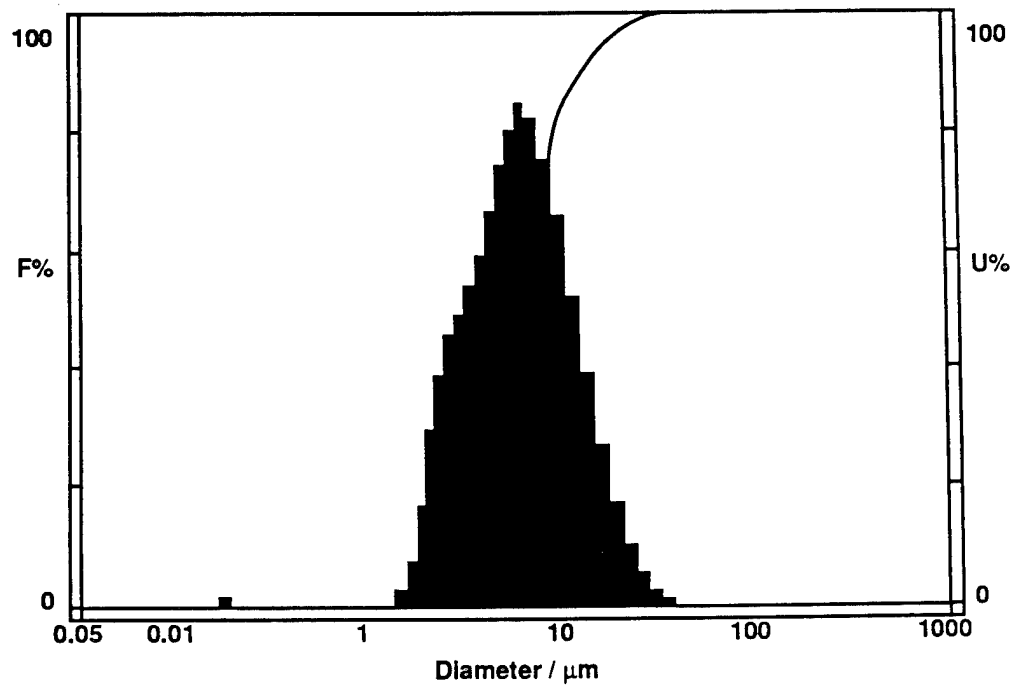

Figure 4.2 Al powder particle size distribution.

found on the Materials Safety Data (MSD) sheet for SiC whiskers [36]. Based on this value samples were exposed to temperatures ranging from 973 to 1173 K for times of one-half hour to two hours in a burnout furnace. The same test was performed with Nb powder at temperatures ranging from 473 to 573 K.

Due to the extremely small size (0.33-1μm diameter) of the SiC whiskers adequate information about the oxide layer was unable to be obtained using an SEM. Therefore, an electron microprobe was selected as an alternate approach to determine the extent of oxidation. Again due to their extremely small size single whiskers could not be isolated for quantitative compositional analysis because of the limits of the equipment. However, relative amounts of oxygen in a clump of whiskers could be distinguished among the different samples. This was done by comparing the oxygen level of the sample to that of the background and reporting the differences. The result of this analysis showed that heating for a period of greater than one half hour and at temperatures between 1073 and 1173 K produced a noticeable oxide layer on the SiC whiskers.

Concurrently, thermal gravitational analysis (TGA) tests were performed to aid in narrowing down the oxidation parameters. These tests were again only able to produce qualitative information. The results of these tests, which are included in the Appendix B, showed that a rapid weight increase (i.e. oxide layer being formed) was noticed on both the 973 and 1073 K runs within the first one half hour. These tests in conjunction with the microprobe results helped narrow down an effective temperature and time range for treating the reinforcements.

With the identification of a temperature range a means by which to produce a uniform oxide layer had to be addressed. In order to achieve a uniform coating it was assumed that the whiskers or particles should be continuously rotated during high temperature exposure. To accomplish this a low cost glass (quartz) reactor was designed (Fig. 4.3) and built to spin inside a tube furnace. The ends of the reactor are supported by and rotate on graphite blocks. A variable speed motor turns the reactor by means of a

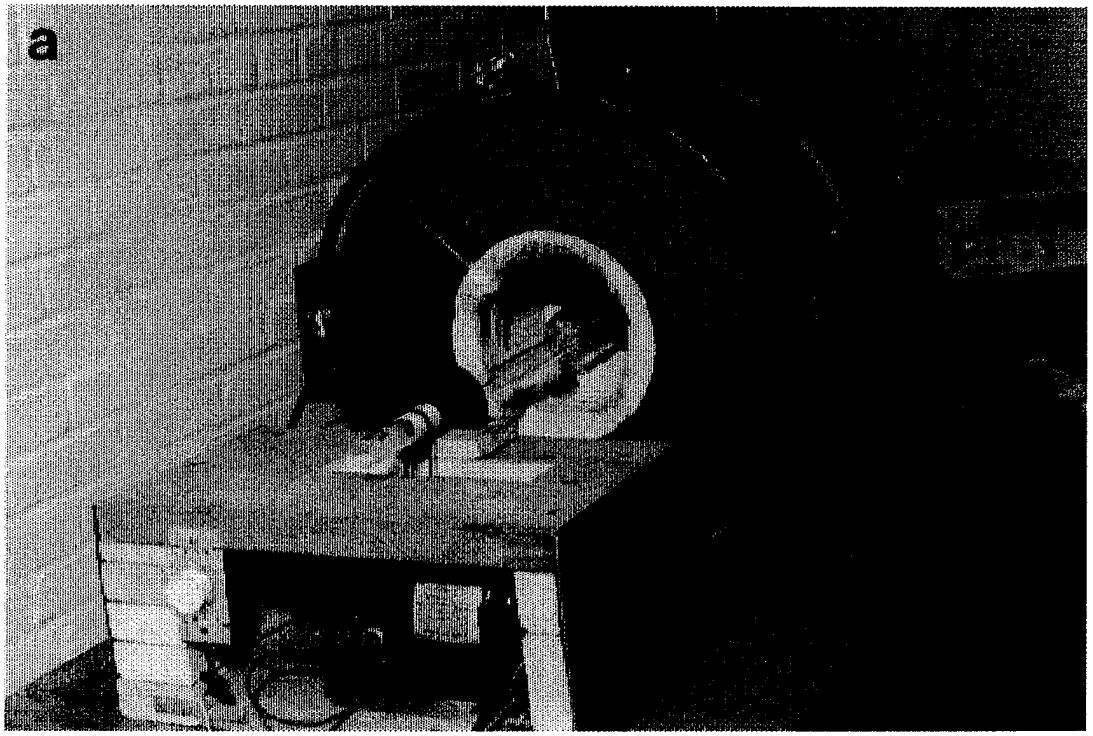

Figure 4.3 Quartz reactor setup showing reactor placement in furnace.

large o-ring. The temperature inside the furnace was monitored with an optical pyrometer and thermocouples. Environmental conditions inside the reaction chamber such as partial pressure of oxygen and humidity could be easily adjusted. Due to temperature limitations of the furnace, 973 K is the maximum allowable oxidation temperature.

It was initially thought that a mixing media (i.e. ceramic mill balls) was needed to break up the whisker clumps. After further examination it was determined that even though the mixing media would help disperse the clumps it would also destroy the brittle oxide layer being produced. Therefore dimples were placed into the reactor (Fig. 4.4) to aid in dispersing the whiskers.

After several experimental runs, varying such things as the rotational speed of the reactor and the volume of whiskers in the chamber, it was concluded that this approach was ineffective. The problem lay in the nature of the SiC whiskers to electrostatically attract to each other. Rotating them in this chamber caused them to agglomerate and form balls ranging from 2 mm to 5 mm in diameter.

Therefore, an alternative approach was taken to treat the reinforcements. They were placed in ceramic tubs and stirred frequently during high temperature exposure in a box furnace. This was advantageous to the fact that higher treatment temperatures could be obtained.

4.3 P/M Processing of Composites

Powder metallurgy (P/M) processing techniques were used for the fabrication of the composites, with consolidation by reaction hot pressing in vacuum. Elemental matrix powders react exothermally and form the niobium aluminide matrix *in situ*. Appropriate quantities of the elemental Nb and Al powders were blended with the reinforcements.

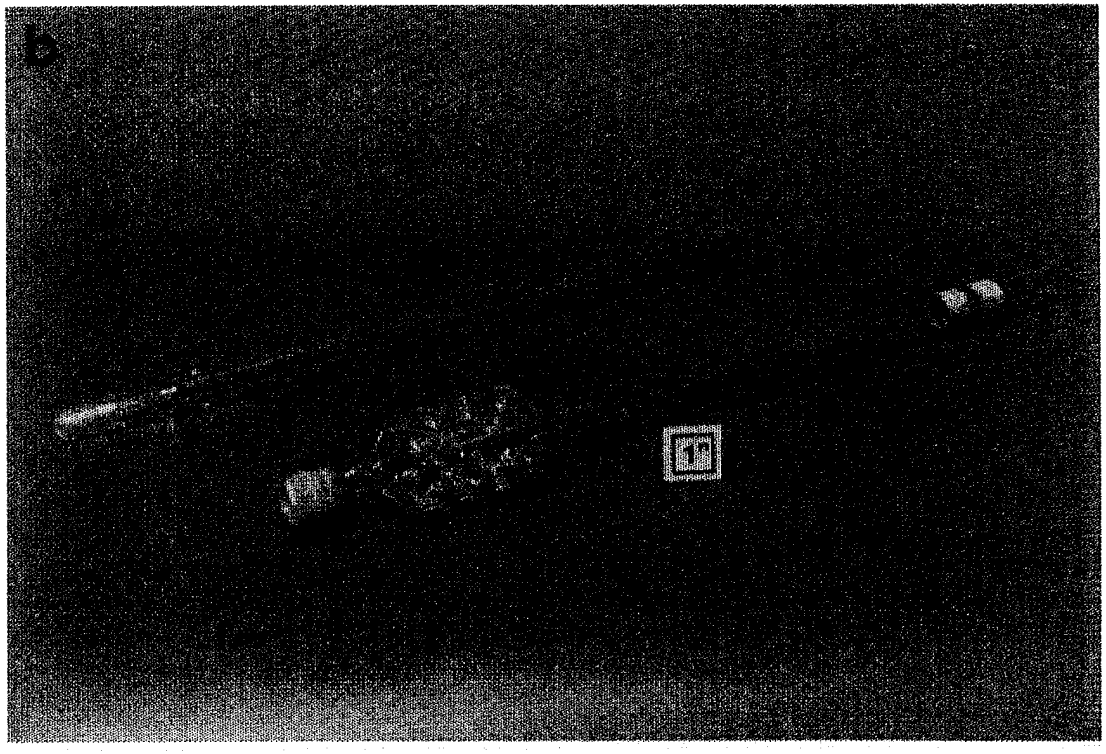

Figure 4.4 Disassembled quartz reactor.

Elemental Nb powder and Al powder were used with M grade SiC whiskers to produce the composites. The blended mix was loaded into a graphite die for subsequent reaction hot pressing in vacuum. The composites were fabricated by consolidating the blended mix under appropriate hot pressing cycles discussed later.

4.3.1 Blending

The powder blending processing step for a composite can have a significant effect on the final properties of the material. Ideally after blending, the powders and the reinforcements would be evenly distributed throughout the material. For this work two types of blending processes were used.

Ball milling of the powders and reinforcements was used to yield adequate blending of the first two composites specimens, those that did not contain treated reinforcements (composites A and B). The powders and reinforcements were added in a 1000 ml plastic bottle that contained 696 grams (174 balls) of 6.35 mm diameter ceramic mill balls and 400 ml of acetone, as the wet mixing media. A wet mixing media was used to reduce the damage to the whiskers and to help disperse the whiskers uniformly throughout the matrix. The slurry was blended for 5 hours and 25 minutes on a horizontal mixer. The acetone was then separated an the remaining powder placed in a drying oven to further remove moisture. To reduce damage to the SiC whiskers and their oxide coating, ball milling was not used for blending the powders of the composites that contained treated reinforcements (composites C and D). The powders and reinforcements for these composites were blended in a Tubula shaker mixer (Type T10-B) for fifteen minutes in an acetone solution. The lack of mill balls and the motion of this device, produced adequate blending with less damage to the reinforcements and their coatings as compared to ball milling. However, large clumps of whiskers that formed as a result of

the oxide treatment remained and proved difficult to disperse. To reduce the amount of whisker clumping in the next composite (composite E) the treated whiskers were placed in an ultrasonic tank before being blended with the matrix powders in the Tubula shaker.

4.3.2 Reaction Hot Pressing in Vacuum

Powder consolidation was accomplished with a vacuum hot press (Fig. 4.5) using graphite dies (Fig. 4.6 and Fig. 4.7) coated with boron nitride to minimize reactions between the powders and the graphite. Hot press cycles for the composites are shown in Fig. 4.8. In selecting a starting temperature for hot pressing it is known that full for density processing, temperatures below approximately one-half the absolute melting temperature is ineffective [37]. With this in mind a maximum starting temperature for the first composite was chosen to be 1673 K. This temperature is 71.7 % of the absolute melting temperature of Nb_3Al (2333 K). The pressure for the system is limited by the material of the dies. The dies, made of graphite, have a maximum strength of approximately 31 MPa (4500 psi). Therefore, in order to stay within the safe operational limits of the tooling a pressure of 27.6 MPa (4000 psi) was initially selected. A vacuum of less than fifteen microns was held on each composite throughout their cycle. During cool down the pressure was removed from the composite at 1273 K and allowed to cool to room temperature overnight.

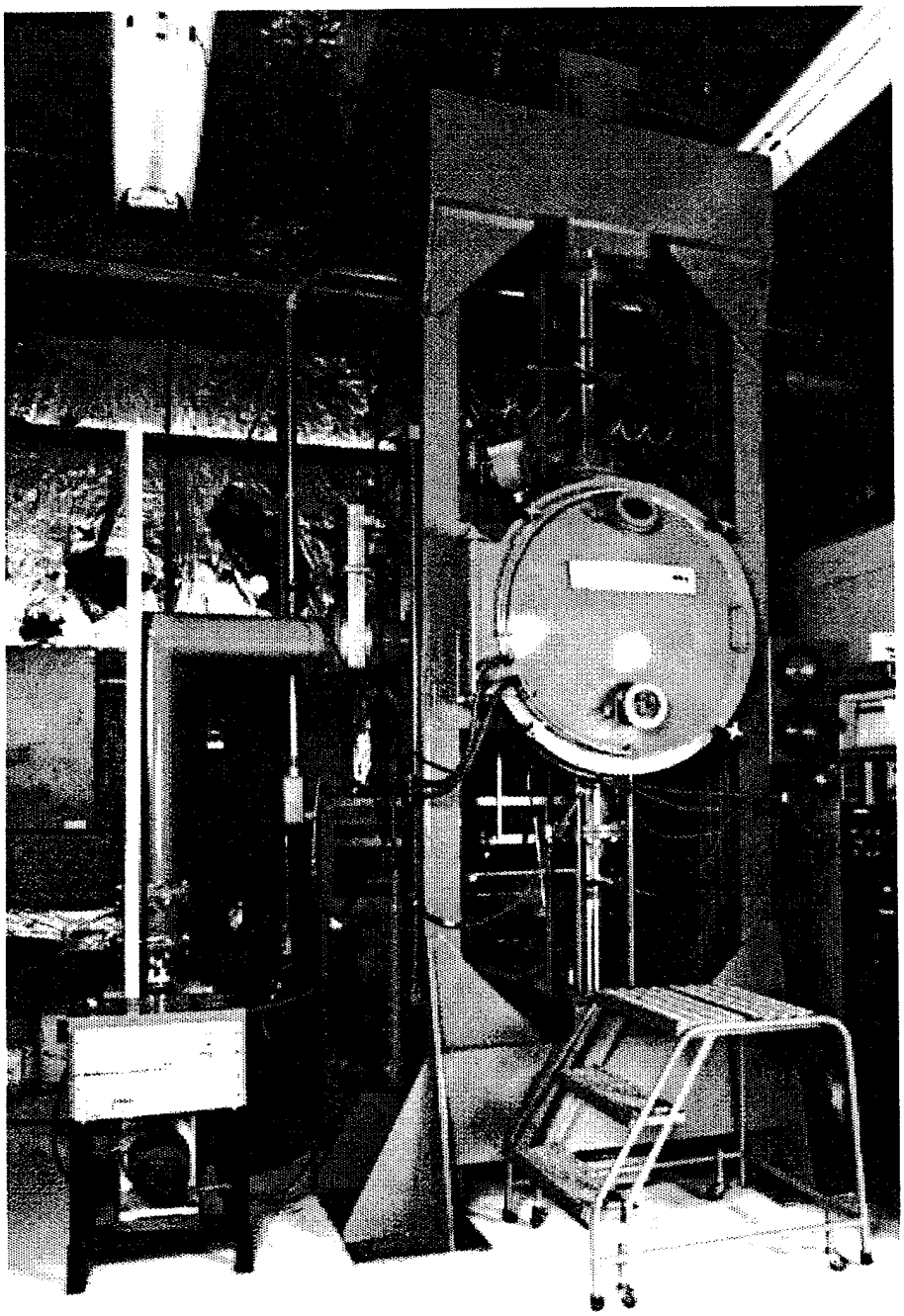

Figure 4.5 Vacuum hot press used to fabricate composites.

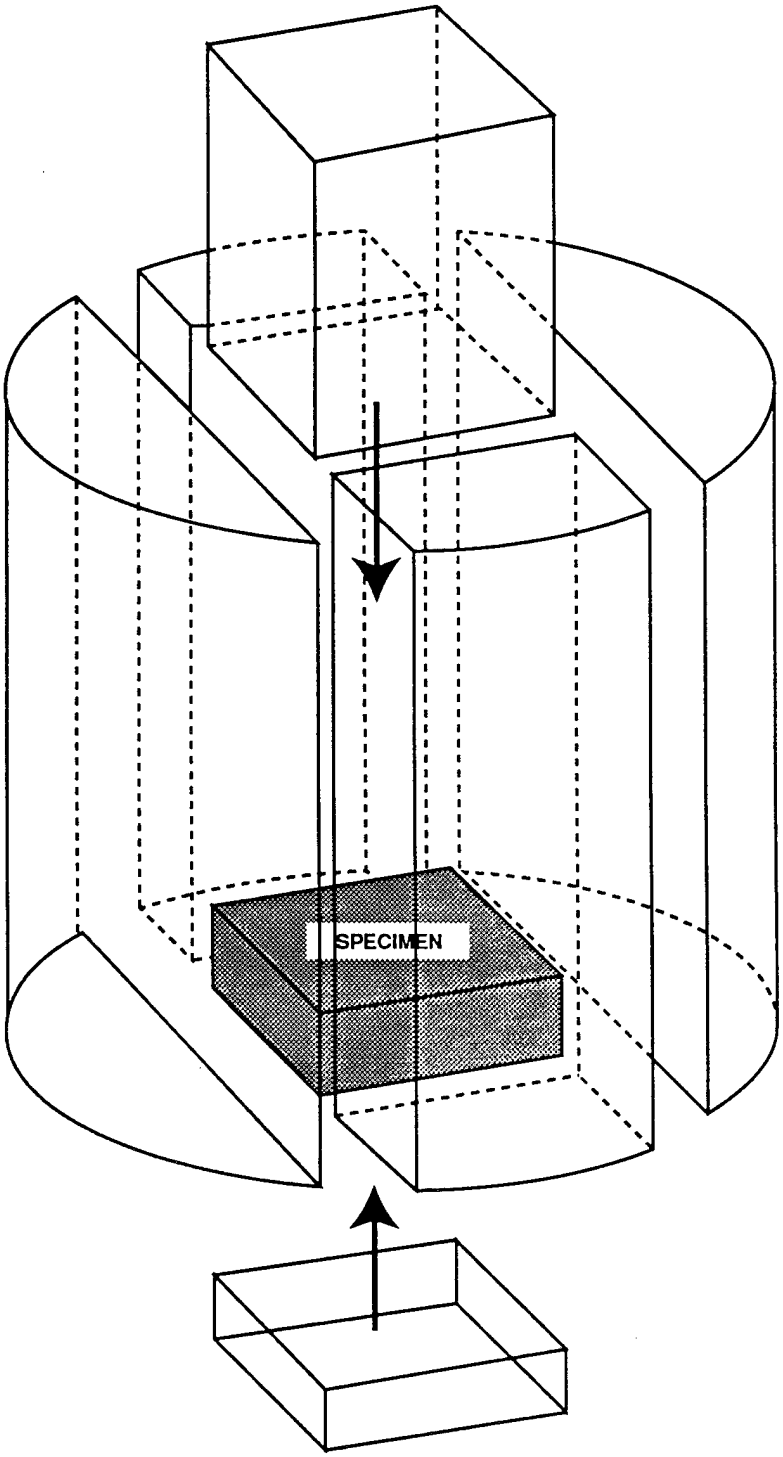

Figure 4.6 Schematic of split graphite die used for reaction hot pressing of composites A and B.

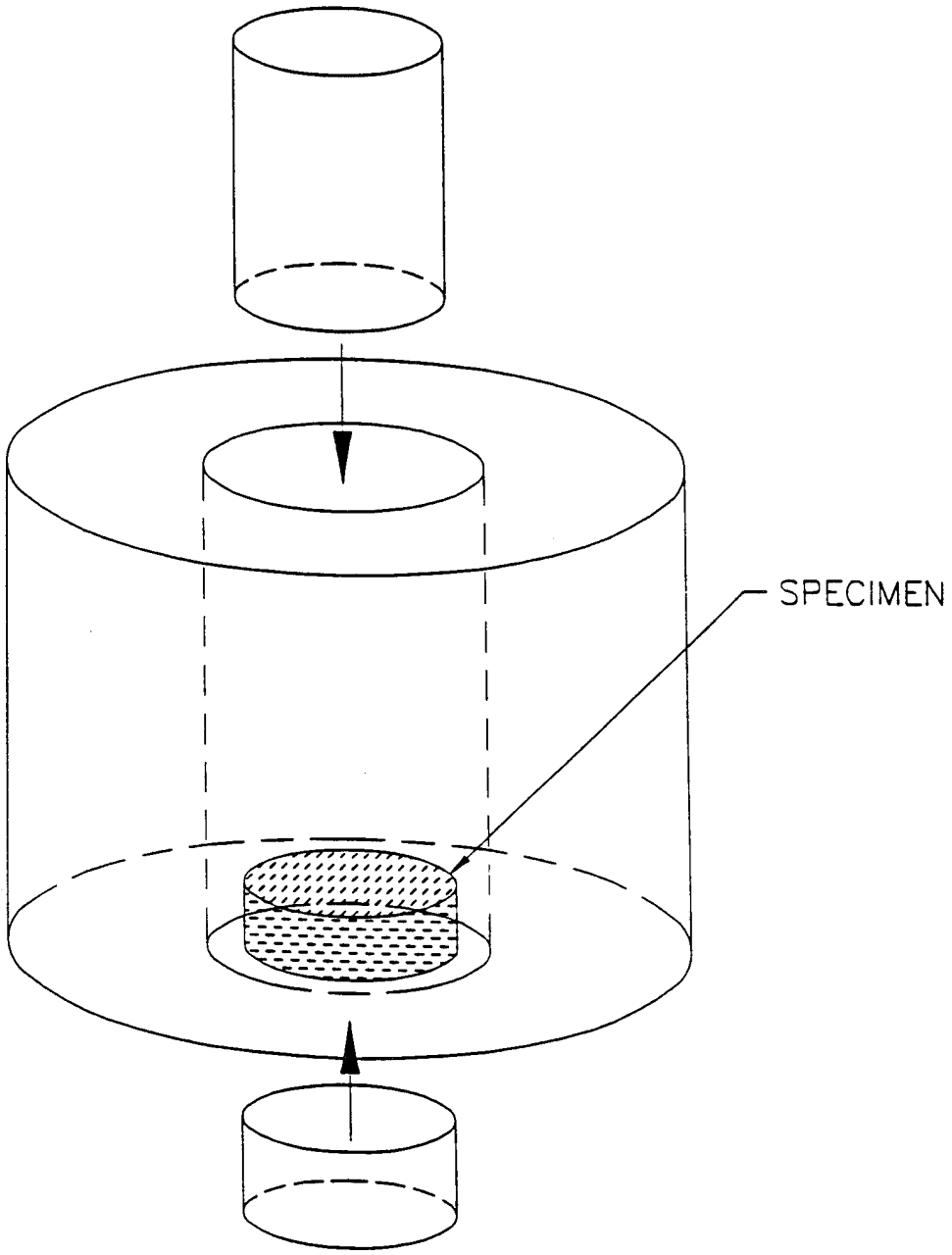

Figure 4.7 Schematic of graphite die used for reaction hot pressing composites C, D and E.

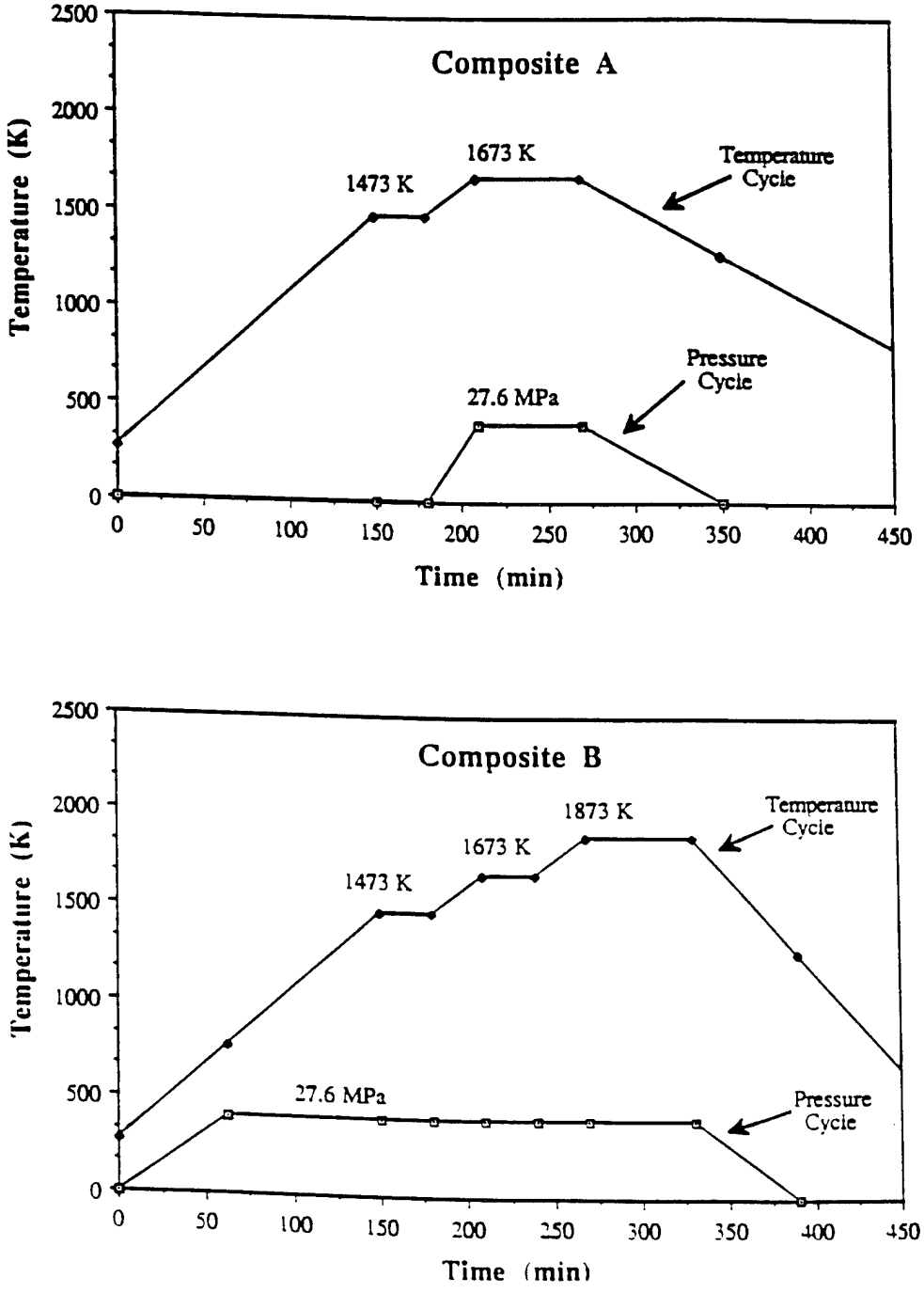

Figure 4.8 a,b. Reaction hot pressing (in vacuum) cycles used for fabricating niobium aluminide matrix composites. (a) Composite A (b) Composite B

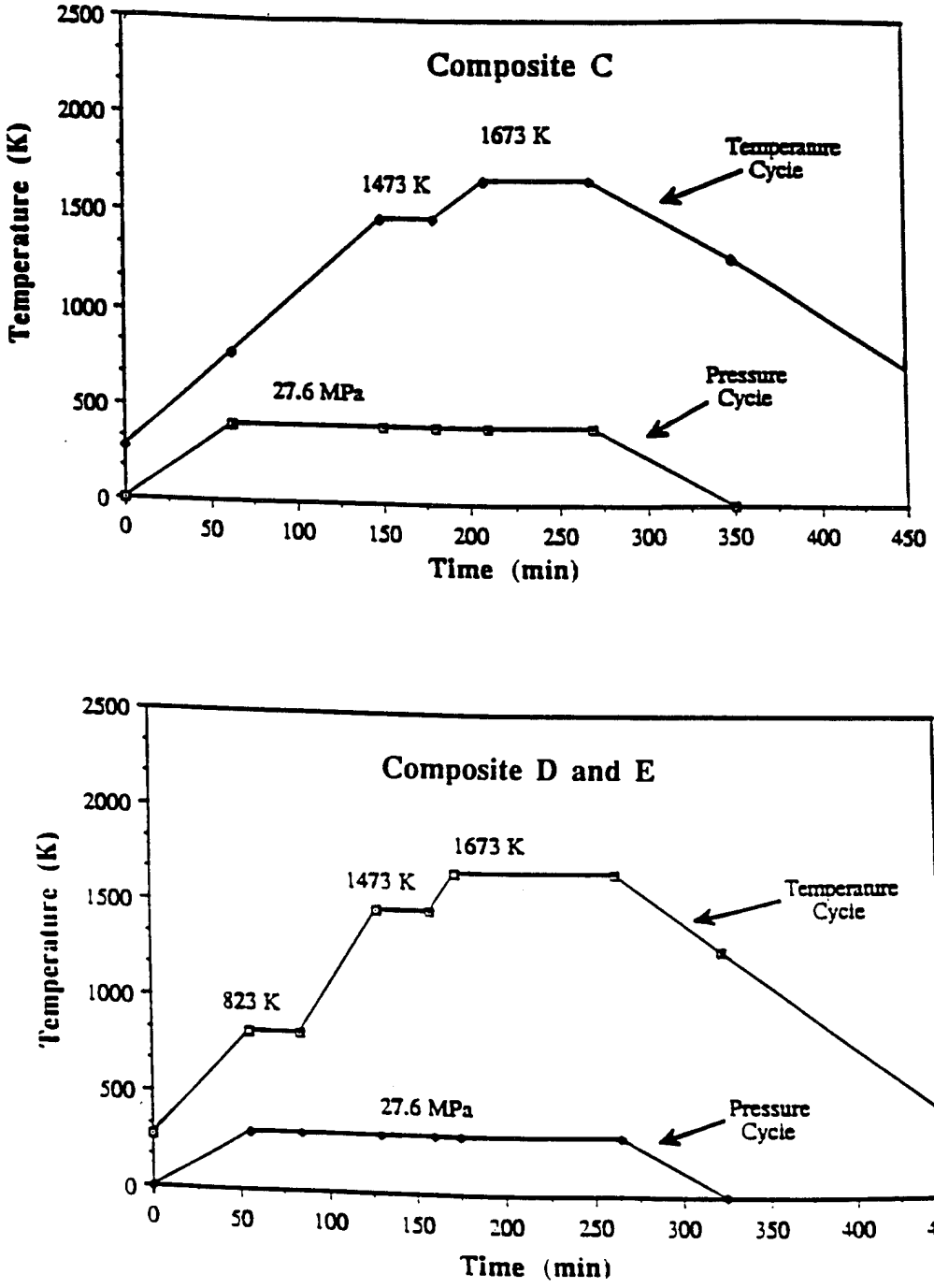

Figure 4.8 c,d. Reaction hot pressing (in vacuum) cycles used for fabricating niobium aluminide matrix composites. (c) Composite C (d) Composites D and E.

Chapter 5

CHARACTERIZATION OF COMPOSITES

The fabricated composites were cleaned and density measurements were taken using the Archimedes principle. Specimens were cut, mounted and polished with diamond paste for microscopy examinations (optical, scanning electron microscope (SEM), and electron microprobe) and microhardness testing. Crack lengths were measured from the hardness indents and were used for fracture toughness comparisons. X-ray diffraction (XRD) was performed on samples from each composite to identify the various reaction products.

5.1 Specimen Preparation

Upon removal from the dies, specimens surfaces were sanded to remove a thin layer of residual powder. The layer resulted from the boron nitride coating that protected the dies. Several samples were then cut from each composite and the density of each was measured. Next, the samples were cold mounted in one inch diameter molds that would allow for polishing. Initial polishing was done with SiC paper with grits ranging from 240 to 4000. Final polishing was done with diamond paste done to a size of 1 μm.

5.2 Density

Density measurements are performed more as a means of comparing the composites to one another, than to compare each to theoretical values. The reason for this is that the theoretical value for Nb_3Al reinforced with 30 vol. % of SiC_w does not take into account the formation of other reaction products, such as: Nb_2Al, $NbAl_3$, Nb_5Si_3, NbC, NbO, etc. which will affect the final density

The density of Nb_3Al obtained from literature is 7.29 g/cc [38]. The density of the composite reinforced with 30 vol. % SiC_w was calculated using equation (1).

$$\rho_c = \rho_f V_f + \rho_m V_m \qquad (1)$$

where, $\rho_f = 3.21$ g/cc (density of SiC_w)

$\rho_m = 7.30$ g/cc (density of Nb_3Al)

$V_f = 0.3$ (volume fraction of SiC_w)

$V_m = 0.7$ (volume fraction of Nb_3Al)

From equation (1) the density of the composite from the rule of mixtures (ROM) is 6.07 g/cc.

To obtain an accurate measurement of the composite density Archimedes Principle was used. Archimedes theory is based on the principle that when a body is submerged in a fluid, a buoyancy force is exerted by the fluid on the body and is equal to the weight of the displaced fluid. The density is calculated according to equation (2).

$$\rho_c = \frac{M_A * \rho_w}{M_A - M_f} \qquad (2)$$

where, M_A is the mass of the specimen in air
M_f is the mass of the specimen suspended in water
ρ_w is the density of water at room temperature

Several samples from each composite were measured and the average of each was calculated and is presented in Table 5.1.

5.3 Hardness

A Vickers micro-hardness test was performed on several samples of each composite to determine its mean hardness. A vickers indentor was used to make a diamond shaped indent on the polished samples. Hardness readings were taken on the bright consolidated regions as shown in Figure 5.1. Due to the relatively small size of the consolidated regions on some samples, maximum loads of only up to .1 kg could be used. Hardness is calculated according to equation (3).

$$H = \frac{P}{2d^2} \tag{3}$$

where, P is the indent load
d is the average diagonal length

The mean hardness values along with the standard deviation for each composite are presented in Table 5.1.

Table 5.1. Properties of the composites fabricated by reaction hot pressing in vacuum, reaction hot pressing cycles are illustrated in Fig. 4.8.

Composite	Initial Composition (wt %)	Density (g/cc)	Microhardness (HV) GPa **		Fracture Toughness Ratio $(N/m)^{1/2}$ ** $K_{Ic}/\xi(E)^{1/2}$	
			mean	std. dev.	mean	std. dev.
A	Nb-77, Al-7, SiC_w-16	5.41	6.6	2.1	–	
B	Nb-77, Al-7, SiC_w-16	6.84	14.5	1.2	277	40
C	Nb-64, Al-6, SiC_w*-16, Nb*-14	4.65	1.9	0.9	314	50
D	Nb-64, Al-6, SiC_w*-16, Nb*-14	4.80	3.5	1.2	–	
E	Nb-64, Al-6, SiC_w*-16, Nb*-14	6.26	2.8	0.8	–	

* These refer to treated reinforcements.

** Of consolidated areas only.

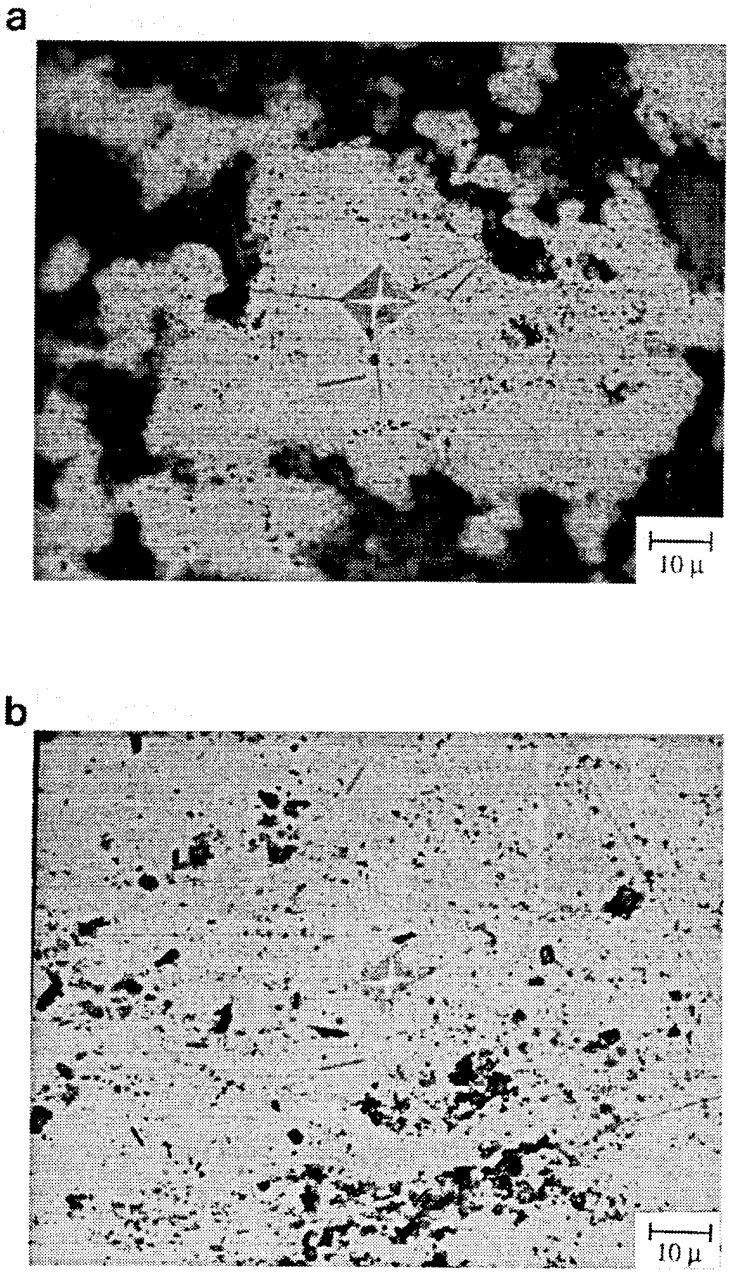

Figure 5.1 a,b. Microhardness indentations on the consolidated regions of composites A and B using a 0.1 kg load. (a) Composite A (b) Composite B

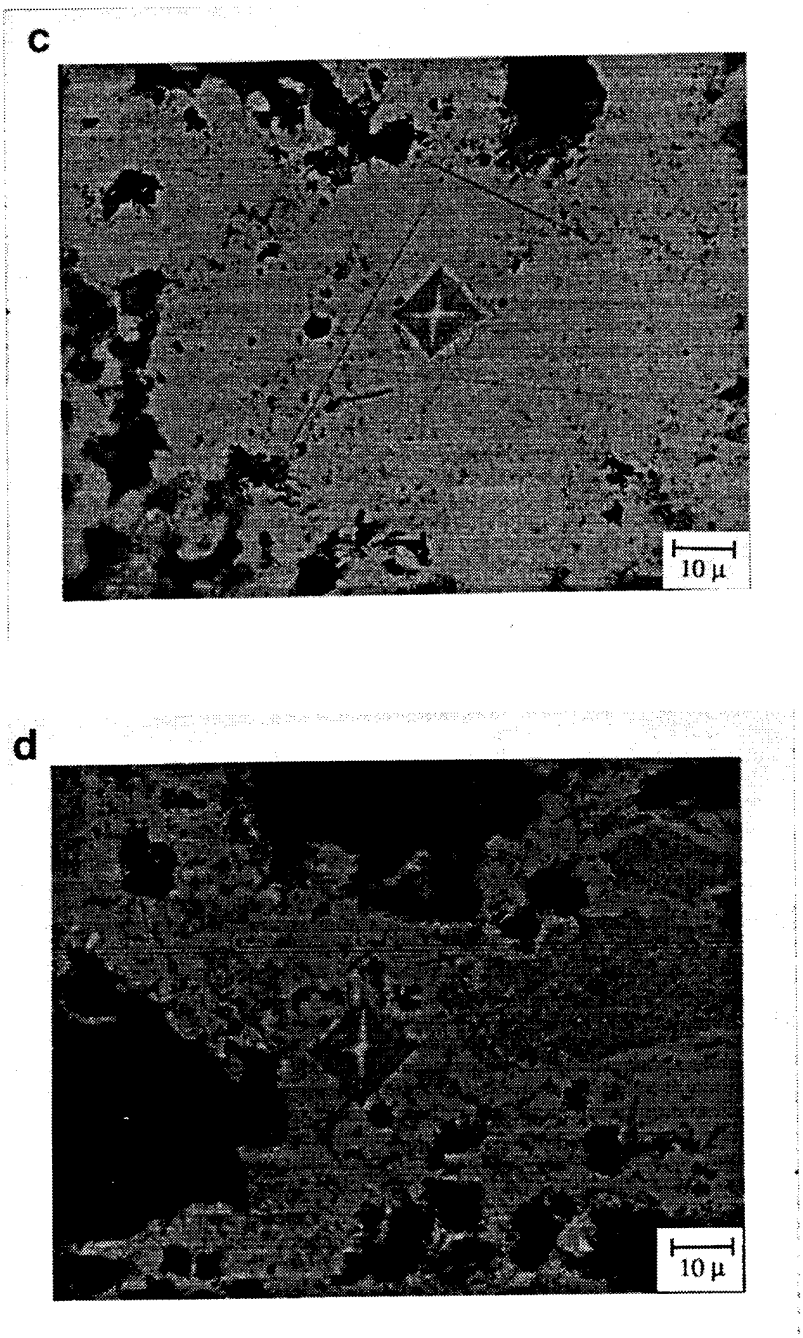

Figure 5.1 c,d. Microhardness indentations on the consolidated regions of composites C and D using a 0.1 kg load. (c) Composite C (d) Composite D

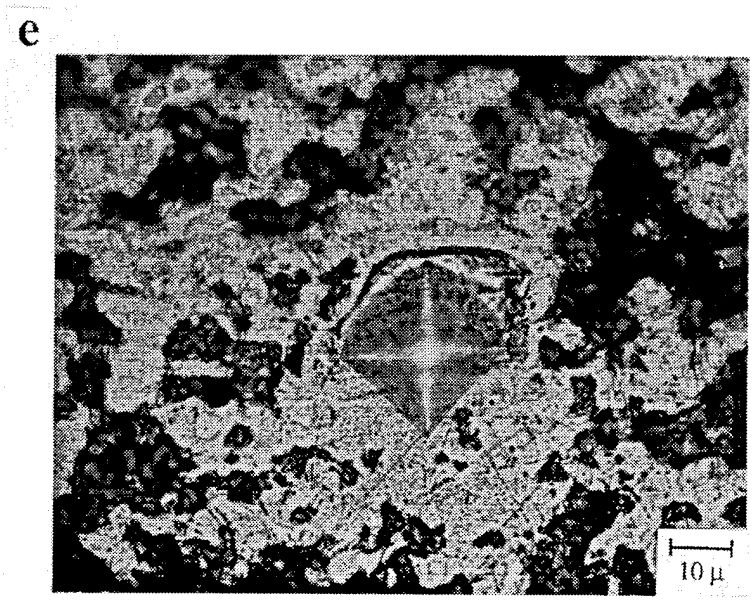

Figure 5.1 e. Microhardness indentation on a consolidated region of composite E using a 0.1 kg load.

5.4 Microstructure

Optical, scanning electron microscope (SEM) and electron microprobe were used to characterize the microstructures. Optical and SEM pictures were taken under a variety of magnifications to visible inspect the microstructures. Detailed compositional analysis was performed on select regions in the microstructure using an electron microprobe. This method identifies the amount of certain elements (by weight percent) in specific regions (Table 5.2 and Fig. 5.2). The microprobe was also used to perform elemental mapping on the composites. Mapping was done for C, O, Al, Nb, and Si (Appendix C). Elemental mapping and compositional analysis allows for a better understanding of what is occurring in the microstructure. Assumptions are then based on this analysis to explain what is occurring during processing. This leads to modifications to optimize the process and therefore improve the composite.

Table 5.2 Microprobe analysis results for the compositions of various regions of composites A, B, and C as marked in Fig. 5.2.

Composite	Labeled Regions	Compositions (wt %)		
		Nb	Al	Si
A	A1	86.4	13.0	0.1
	A2	95.8	0.06	0.01
	A3	57.0	41.0	0.3
B	B1	70.0	5.2	22.3
	B2	83.0	1.4	13.9
C	C2	100.0	0.0	0.0
	C3	93.2	6.2	0.3
	C4	87.7	11.6	0.2
	C5	82.0	5.7	8.3

a

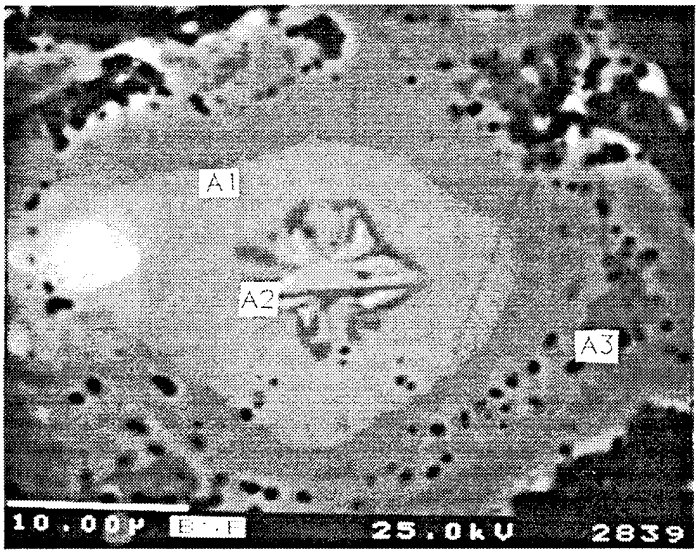

b

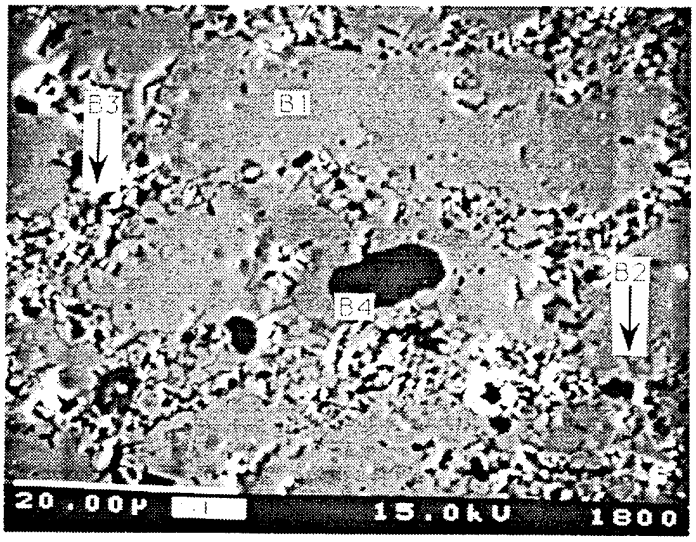

Figure 5.2 a, b SEM micrograph of composites A and B showing compositional inhomogeneity: compositions of labeled regions for composites A and B, determined by microprobe, are included in Table 5.2. (a) Composite A (b) Composite B

c

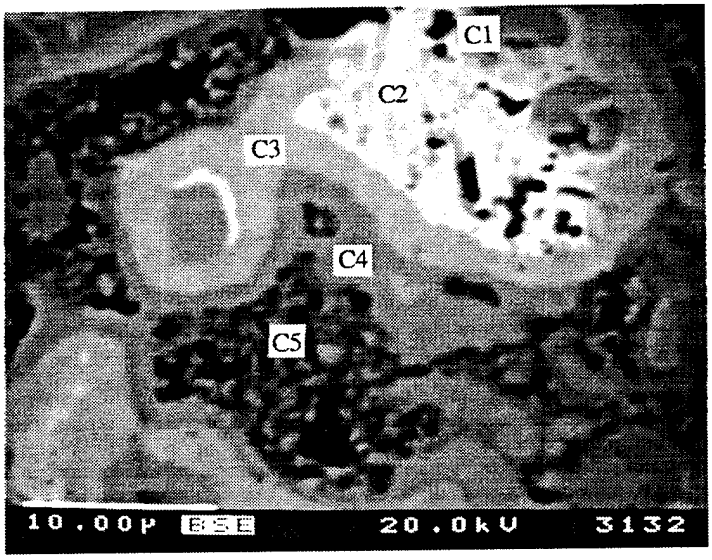

Figure 5.2 c. SEM micrograph of composite C showing compositional inhomogeneity: compositions of labeled regions determined by microprobe, are included in Table 5.2.

5.5 X-ray Diffraction (XRD)

The fact that every element / compound either alone or in the presence of others produces a characteristic diffraction pattern, is the basis for chemical analysis by x-ray diffraction (XRD). XRD actually identifies the chemical combinations of elements present in a specimen whereas other chemical analysis techniques only identify the presence of element A or B. X-rays are generated when accelerated electrons, generated by a cathode, strike an anode. These x-rays are directed toward and strike the surface of the specimen where they interact with the material according to wave theory. The x-rays are reflected or diffracted at particular angles (Bragg) according to the lattice spacing of a specific phase. The pattern produced (Fig. 5.3) can then be compared to known data to determine the phase or phases present. The results of this analysis were used to verify microprobe analysis and provide a better understanding of events occurring during processing. Table 5.3 contains the phases identified ineach composite.

Table 5.3 Phases identified in each composite using XRD techniques.

Composite	*XRD*
A	Nb_3Al, Nb_2Al, NbC, SiC, Nb
B	Nb_5Si_3, Nb_3Si, NbC, SiC
C	Nb_3Al, Nb_2Al, NbC, Nb, SiC
D	Nb_3Al, Nb_2Al, NbC, NbO, Nb, SiC
E	Nb_3Al, Nb_2Al, NbC, NbO, Nb, SiC

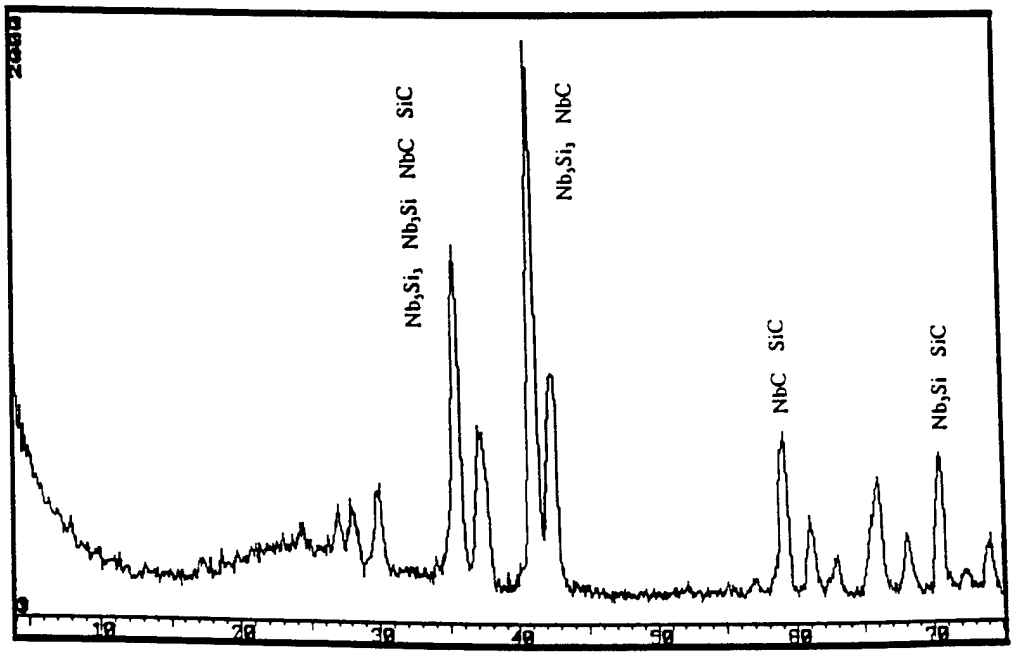

Figure 5.3 X-ray diffraction pattern of composite B.

5.6 Ultrasonic C-Scan

An ultrasonic C-scan was performed to identify defects (voids, cracks or density gradients) within a composite. A 30 Mhz transducer with a 19.05 mm (3/4 inch) focal length was used. Eight gates were set through the thickness of the composite in order to acquire information at various depths. A scan of the whole 50.8 mm x 50.8 mm (2" x 2") composite was first performed (Fig. 5.4) and then the scanning area was reduced to 10.2 mm x 10.2 mm (0.4 " x 0.4") (Fig. 5.5) in order to increase the resolution of the scan. No unusual or *gross* defects were observed from these scans. Velocity measurements were also taken throughout the composite to aid in identifying density gradients. The time for a pulse (wave) to go down through the sample and back was measured and recorded in micro-seconds. These times were compared with others measured throughout the sample and the results showed no *gross* variation in density across the specimen.

5.7 Fracture Toughness by Indentation

Measuring or estimating the fracture toughness of brittle materials, such as ceramics or intermetallics by the Vickers microhardness indentation method has been widely applied and accepted for more than a decade. The cracks produced by the microhardness indentations were used to determine an apparent fracture toughness ratio for composites B and C. Small size of the consolidated regions precluded such determinations for composites A, D, and E. Fracture toughness can be calculated directly from the crack lengths of hardness indentations (see the schematic in Fig. 5.6) using Eqn (4) [39]:

$$K_{Ic} = \xi\left(\frac{E}{H}\right)^{1/2} \frac{P}{c^{3/2}} \qquad (4)$$

where, K_{Ic} = mode I fracture toughness P = indent load

E = Young's modulus c = half crack length

H = hardness ξ = material independent constant

Table 5.1 includes the calculated fracture toughness ratios obtained from Eqn. (4). Composite B was indented with a load of 1 kg to produce radial cracks (Fig. 5.7), but a smaller load of 0.1 kg had to be used for composite C due to the relatively small size of the consolidated regions. It was assumed that the constant ξ has the same value for both composites and that the consolidated regions of both composites have the same stiffness. Since the composites are not fully consolidated, no attempt has been made to determine the pertinent values of ξ and E.

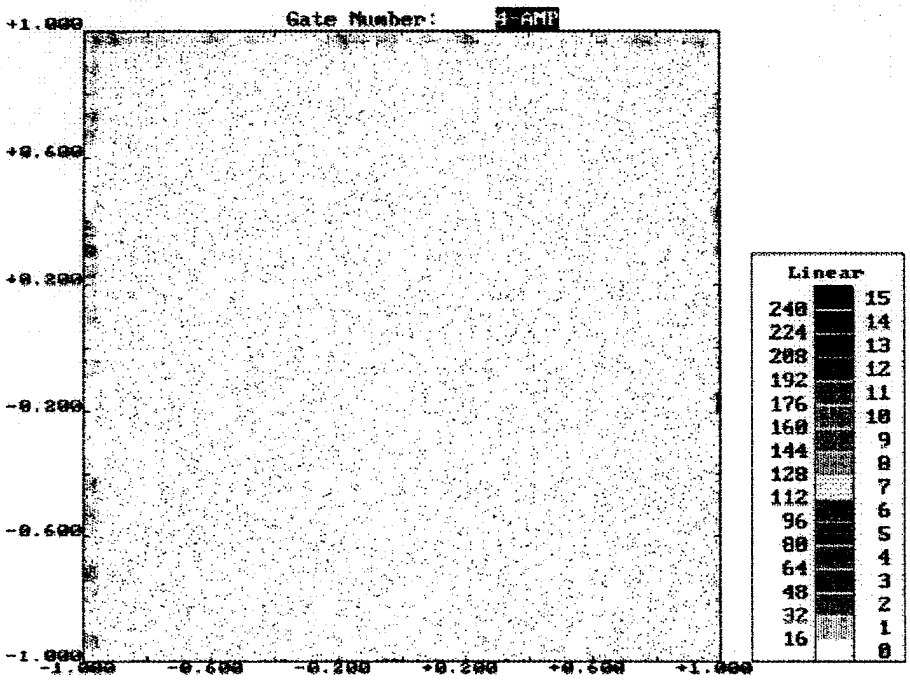

Figure 5.4 Ultrasonic C-scan of entire (50.5 mm x 50.8 mm) composite A, using a 30 Mhz transducer with a 19.05 mm focal length.

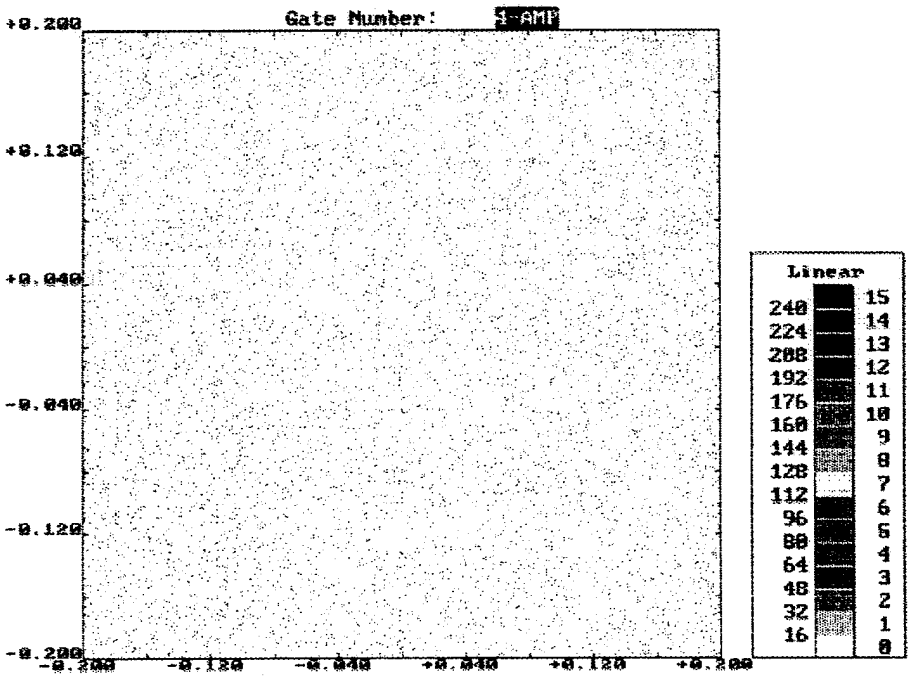

Figure 5.5 Ultrasonic C-scan of a reduced region (10.2 mm x 10.2 mm) on composite A, using a 30 Mhz transducer with a 19.05 mm focal length.

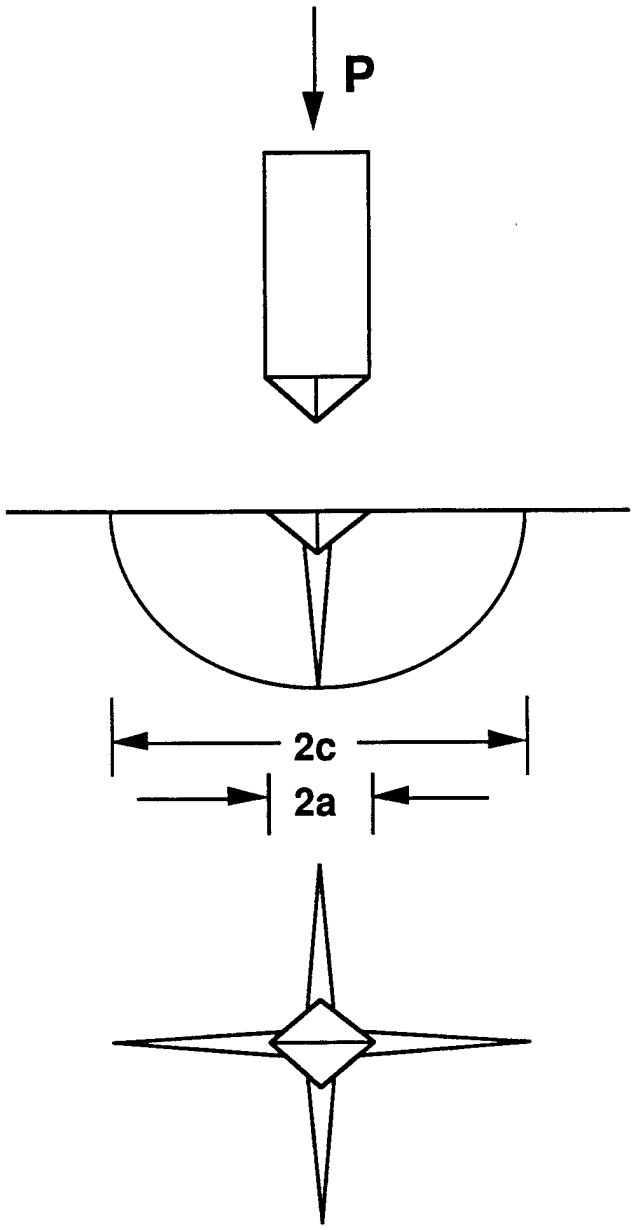

Figure 5.6 Schematic of indentation-fracture system, peak load P, showing characteristic dimensions c and a of penny-like radial / median crack and indent impression, respectively [39].

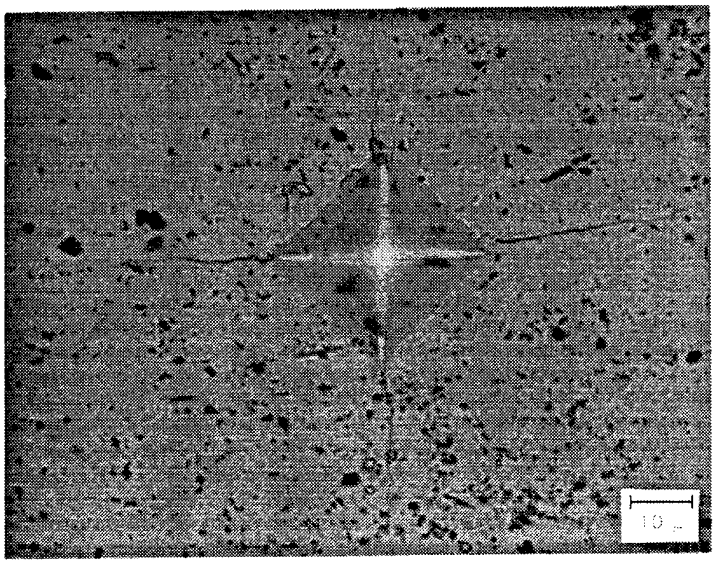

Figure 5.7 Microhardness indentation (1 kg load) in composite B showing radial cracks that are used in determining the fracture toughness of the consolidated regions.

Chapter 6

RESULTS AND DISCUSSION

Five composites were fabricated at the completion of this study. Two that contained untreated reinforcements (composites A and B) and three that contained treated reinforcements (composites C, D, and E). Initial compositions prior to the reaction hot pressing are included in Table 5.1. The density and hardness of the fabricated composites, designated as A, B, C, D, and E also are included in Table 5.1. The hot pressing cycle corresponding to each composite is shown in Fig. 4.8. Changes were made to each hot pressing cycle following the characterization of prior composites toward achieving greater densification. Low magnification optical micrographs (Fig. 6.1) of each composite show the extent of consolidation.

Composite B has the highest density and shows the largest amount of consolidated areas as a result of: (a) a higher hot pressing temperature (1873 K) (see Fig. 4.8b), and (b) the degradation of the SiC whiskers. Detailed compositional analysis performed on composite B (see Table 5.2) led to the identification of several areas of interest as shown in Fig. 5.2b. One region that made up the bulk of the material consisted of Nb and Si close to the composition of Nb_5Si_3. Another region contained large amounts of niobium carbide. The presence of SiC whiskers in the microstructure could not be confirmed. Based on these findings it was concluded that the SiC whiskers reacted with the matrix materials to form niobium carbide and niobium silicide. XRD was performed on the composite and its results (Table 5.3) agreed with the microprobe analysis.

With the addition of the treated reinforcements a substantial decrease was observed in the hardness and an increase was observed in the fracture toughness of composite C as seen in Table 5.1. The results showed an increase of 15% in the mean

a

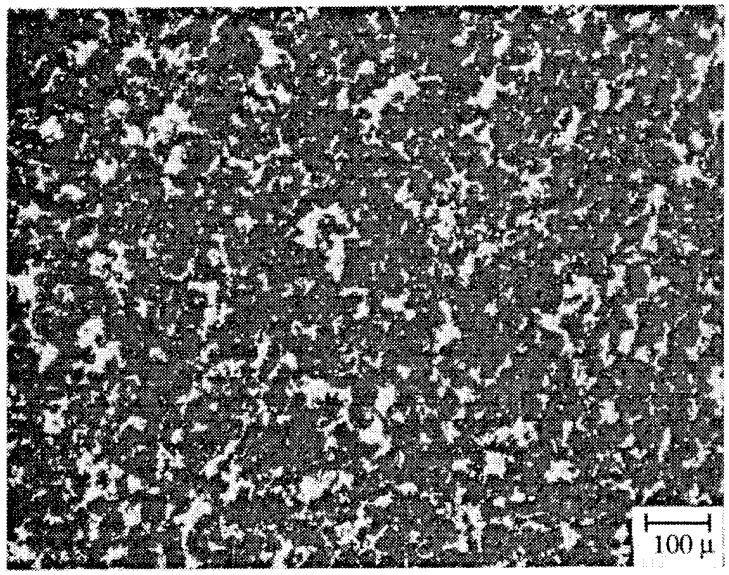

b

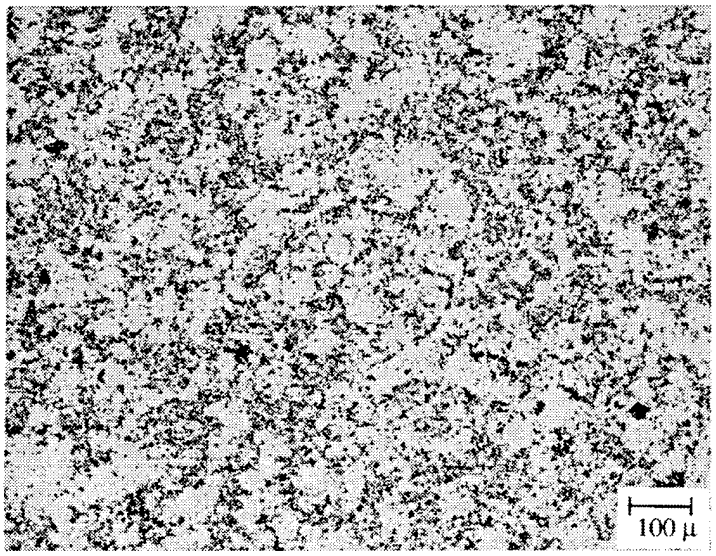

Figure 6.1 a,b Optical micrographs illustrating the extent of consolidation in each composite. Light areas represent fully consolidated regions while the dark areas represent poorly consolidated regions. (a) Composite A (b) composite B.

c

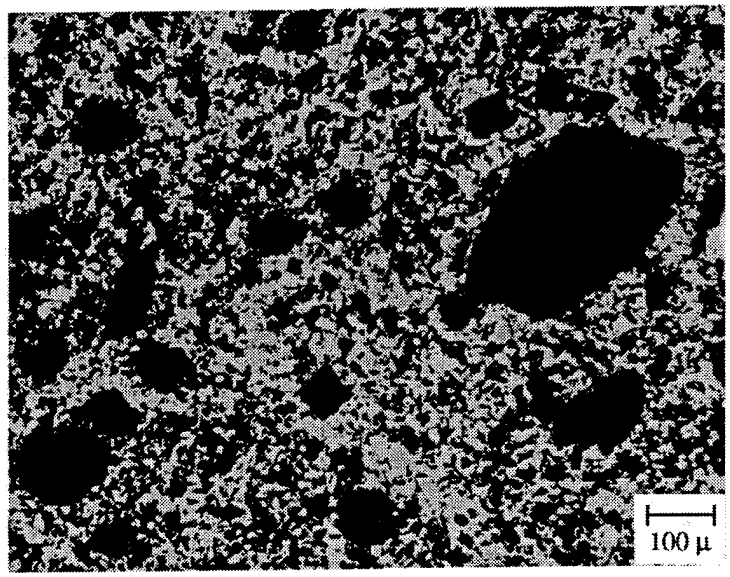

d

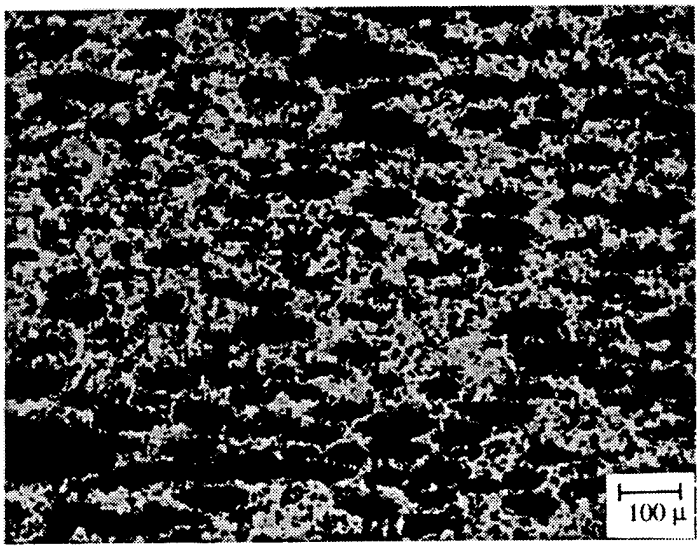

Figure 6.1 c,d Optical micrographs illustrating the extent of consolidation in each composite. Light areas represent fully consolidated regions while the dark areas represent poorly consolidated regions. (c) Composite C (d) composite D.

e

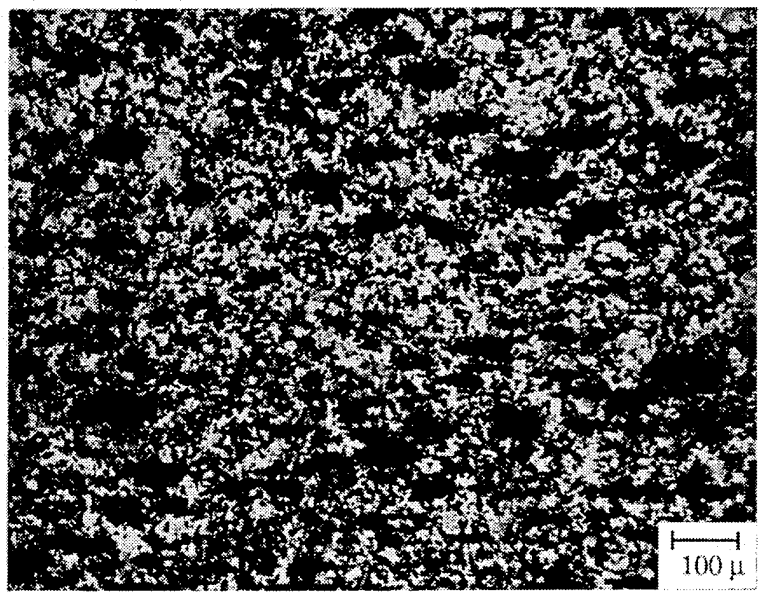

Figure 6.1 e Optical micrograph illustrating the extent of consolidation in composite E. Light areas represent fully consolidated regions while the dark areas represent poorly consolidated regions.

fracture toughness of composite C, containing the treated reinforcements, relative to that of composite B. The comparatively high fracture toughness of the consolidated region in composite C is consistent with microstructural observation of plastic deformation (Fig. 6.2) at the indentations and relatively low hardness. This composite contained both treated SiC whiskers and treated Nb particles. The treatment reduced the degradation of the reinforcements by the matrix materials. However, since no whiskers were identified in the reacted material of composite C and niobium carbide was detected during characterization it was assumed that the oxide layer was not sufficient to totally protect the whiskers from reacting with the elemental Nb during the reaction hot pressing. Therefore, for the next composite (composite D) the treatment temperature for the whiskers was increased, consistent with the work of Ribes et al. [40], who reported an approximate 50 nm thick oxide layer on SiC particles after treatment for two hours at 1373 K. Also a degassing step was added prior to hot pressing to remove absorbed species from the powders. The powder blend was degassed at 773 K for six hours. The hot pressing pressure cycle remained unchanged but several changes were made to the temperature cycle for fabricating composite D (Fig. 4.8d). These changes reflected the potential temperature range (1023 to 1173 K) for the exothermic reaction that takes place between Nb and Al [41, 42]. A 30 minute hold time was used at 823 K to ensure a uniform sample temperature. Above this temperature when the exothermic reaction is expected to occur, the temperature of the sample may increase substantially (several hundred degrees) for a short time period as the molten Al reacts with the solid Nb particles to form one or more intermetallic compounds. The heat rise is expected to sustain the reaction until all of the starting elemental powders are used up. Following the exothermic reaction the temperature recedes and further densification is accomplished by hot pressing at higher temperatures and pressures. Therefore, the heating rate was increased to reduce hot pressing time and consequently reducing reinforcement exposure time to elevated temperatures.

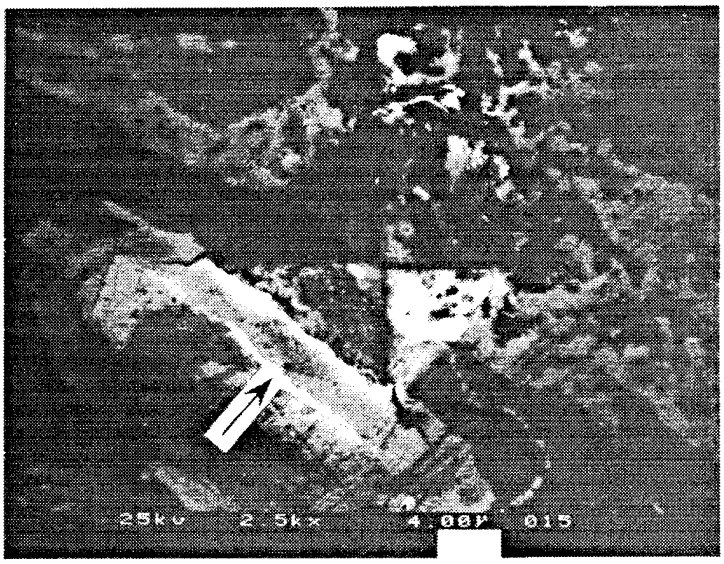

Figure 6.2 Microhardness indentation in composite C, using a 0.1 kg load, showing a regon of local yielding.

The consolidation of composite D improved over composite C as shown by the 3.20 % increase in density (Table 5.1). The XRD pattern for this composite (Fig. 6.3a) matched very well with a pattern produced by Murugesh et al. [43] for hot pressed Nb_3Al (Fig. 6.3b). However, some poorly consolidated regions consisting mostly of SiC whiskers are visible in the SEM micrographs of composite D as well as composite C (Fig. 6.4). This is attributed to whisker-to-whisker bonding that may have taken place between the whiskers during the oxide treatment. This results in poor dispersion of the whiskers into the matrix during blending.

An additional blending step was added for the fabrication of the next composite (composite E) to help disperse the whisker clumps. After treatment the whiskers were placed in an ultrasonic bath for several hours prior to blending with the matrix powders. The high frequency vibration of the bath is expected to shake loose bonded whiskers without damaging the coating. The hot press cycle for this composite remained unchanged from the previous composite (Fig. 4.8 d). Following consolidation fewer large clumps of whiskers are observed in the unconsolidated regions of composite E compared to composite D as viewed in the optical micrographs (Fig. 6.1 d and Fig. 6.1 e). Also, the poorly consolidated regions that do exist in composite E appear to be more consolidated than previous composites (Fig. 6.5). Composite E has the highest density of the composites containing treated reinforcements and a hardness substantially lower with less scatter than composites containing untreated reinforcements (Table 5.1). Based on these results and those of composites C and D, it is deemed appropriate to suggest that the room temperature ductility/toughness can be substantially improved by incorporating treated reinforcements into niobium aluminide matrix composites.

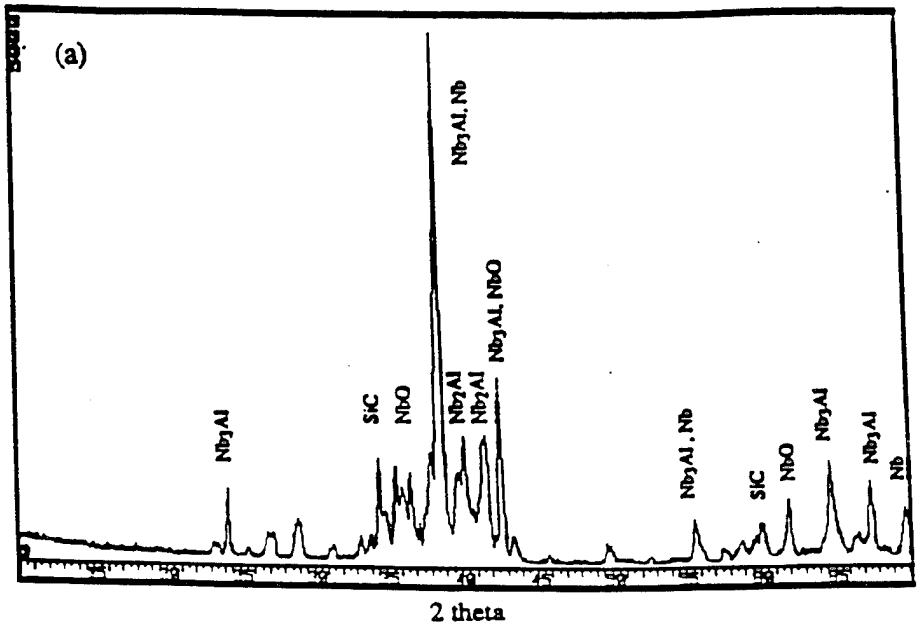

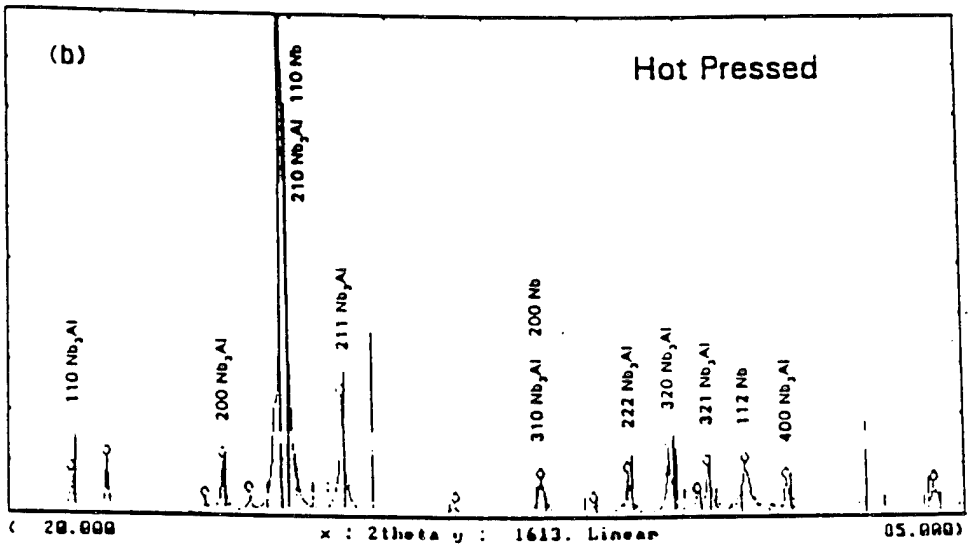

Figure 6.3 a) X-ray diffraction pattern of composite D. b) X-ray diffraction pattern from literature for niobium aluminide system (Murugesh et al. [43]).

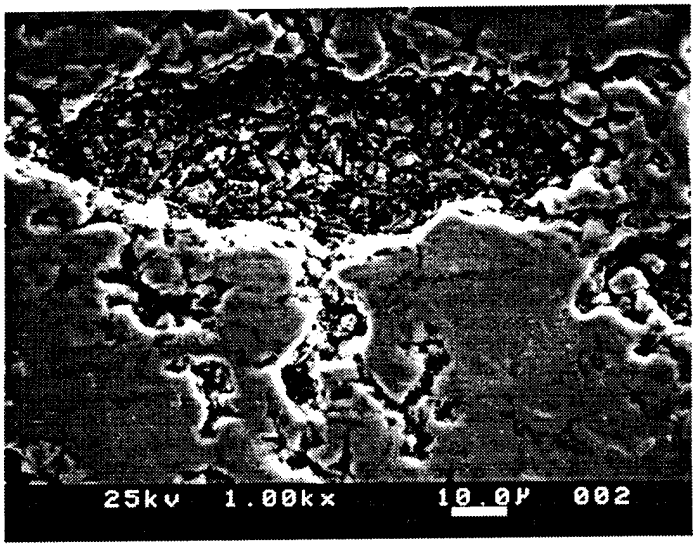

Figure 6.4 SEM micrograph of composite D. Fully consolidated and poorly consolidated regions are seen.

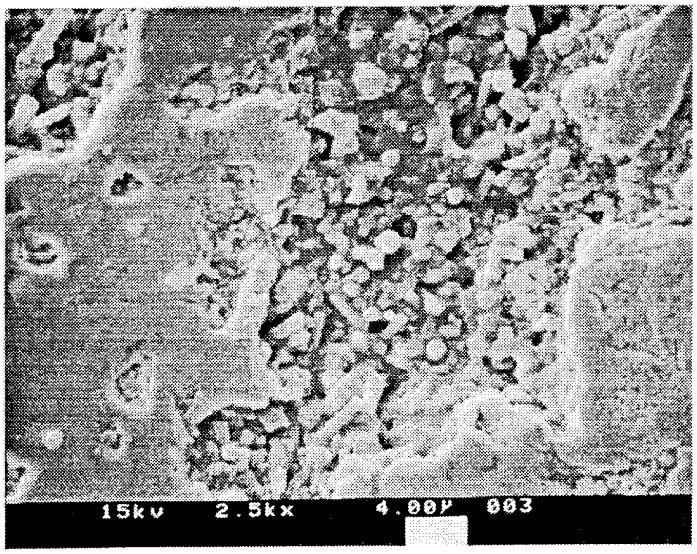

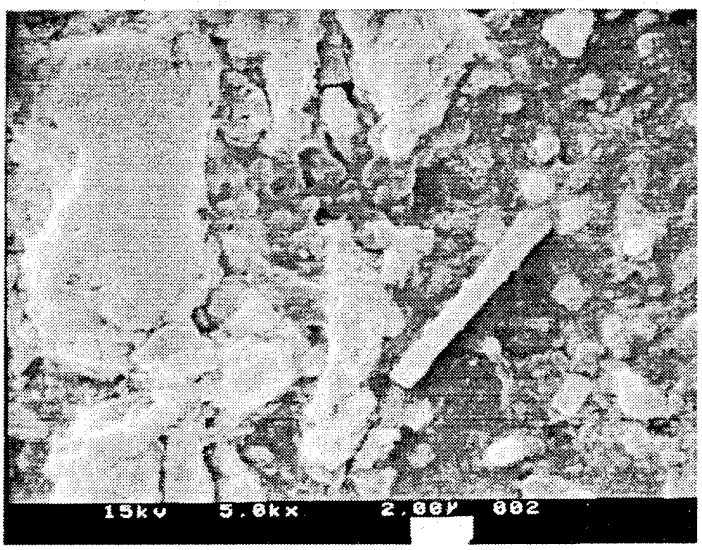

Figure 6.5 a,b. SEM micrographs of composite E showing fully consolidated regions and partially consolidated regions. SiC whiskers can be seen surrounded by matrix material.

Chapter 7

SUMMARY AND CONCLUSIONS

Discontinuously reinforced niobium aluminide matrix composites have been fabricated by reaction hot pressing in vacuum. The intermetallic matrix is formed *in situ* during the processing. A hot pressing cycle has been established for the successful fabrication of the niobium aluminide matrix, while reducing adverse reactions between the treated reinforcements (Nb and SiC_w) and the matrix. A thermodynamic study using SOLGASMIX suggests that the "treated" reinforcements are likely to be protected from an adverse reaction with the matrix during the exothermic reaction between elemental niobium and aluminum powders and subsequently with the niobium aluminide matrix during processing. Thus, the fabricated composites are expected to be thermally stable when exposed to elevated temperatures. Also, these composites are expected to have favorable characteristics of the interfaces for improved fracture toughness at room or low temperatures.

Microscopy examinations (optical, SEM, and microprobe), and x-ray diffraction (XRD) analysis were used to characterize the fabricated composites. Microprobe and XRD analysis were used to identify the intermetallic phases and other reaction products present in each composite. A more detailed analysis of the characterized composites is included in reference [44]. The fabricated composites exhibited consolidated regions along with the presence of some unconsolidated regions. Optimization of the processing parameters led to increased densification of the composites; however, the presence of certain pockets of unconsolidated regions could not be completely eliminated. Further process optimization is recommended. Nevertheless, characterizations of the fabricated composites offer valuable insight into understanding the consolidation of the elemental matrix powders with two reinforcement materials (treated or untreated).

Room temperature fracture toughness of the consolidated regions was calculated using the indentation method. Table 5.1 contains the fracture toughness results in terms of a ratio along with the initial composition, density, and hardness for four composites. Lower hardness and higher fracture toughness were observed in the composite containing "treated" reinforcements (composites C, D, and E) in comparison to the composites with untreated reinforcements (composites A and B). Therefore, based on the microstructural characteristics, microhardness and the apparent mode I fracture toughness (determined by indentation method) it is concluded that the use of oxide-coated silicon carbide whiskers and niobium particles as reinforcements leads to an improvement (15 %) in fracture toughness of the composite in comparison with the untreated SiC_w reinforced composite. The optimization of the coating on the reinforcements and the reaction hot pressing is likely to improve the room temperature fracture toughness further.

Chapter 8

RECOMMENDATIONS FOR FUTURE STUDY

This study touched on many areas in the fabrication and characterization of niobium aluminide based composites. However, due to time and resource limitations some areas were unable to be fully investigated in the scope of this study. Further work in several of these areas is recommended to better understand and improve the processing.

Additional work should focus primarily on improving the densification of the composite. Once full densification is achieved mechanical testing can be performed to determine the material properties and validate the results of this preliminary study. The elastic modulus, once determined, can be used to calculate the composite's fracture toughness by the indentation technique. Full densification will allow larger indent loads to be used which will create larger cracks. This will reduce the effects that individual whiskers and particles have on the cracks and allow for reproducible K_{ic} values. Full densification of the composite will also allow for elevated temperature creep tests that are needed to evaluate our hypothesis of improved creep resistance.

This study showed that ultrasonic blending of the treated whisker reinforcements improved the final composite's density. Further improvement in the composite could be achieved with optimization in this area. Tests could be performed at different frequencies and times to achieve optimal whisker dispersion.

Further work is also needed to improve the treatment process as well as to characterize the thickness of the oxide layer produced. The treatment process should be improved to achieve a uniform or near uniform layer on the SiC whiskers. Other treatment processes should be considered.

REFERENCES

1. D.L. Anton, D. M. Shah, D. N. Duhn and A. F. Giamei, J Metals, 12-17 (Sept. 1989)
2. J. H. Westbrook, Structural Intermetallics, 6 (1993)
3. T. H. Courtney, "Mechanical Behavior of Materials", 119 (1990)
4. U. R. Kattner, Binary Alloy Phase Diagrams, 180 (1990)
5. C.T. Liu, Sci. Advanced Maters, 423-459 (1988)
6. Erland M. Schulson, Intrn. J. Powd. Metall., **23**, No. 1, 25-32 (1987)
7. D. L. Anton, and D. M. Shah, in High Temperature Structural Intermetallic Compounds, (edited by C.T. Liu et al.), MRS, Pittsburgh, PA, 361 (1989)
8. C. T. Liu, and K. S. Kumar, J Metals, **45**, 38-44 (1993)
9. M. F. Amateau, and R. B. Bhagat, Advances in Powder Metallurgy & Particulate Materials, Metal Powder Industries Federation, New Jersey , 223-236 (1992)
10. K. S. Kumar, and C. T. Liu, J Metals, **45**, 28-34 (1993)
11. A. K. Vasudevan, and J. J. Petrovic, Mater. Sci. Engng, **A155**, 1-17 (1992)
12. K. Sadananda, and C. R. Feng, J Metals, **45**, 45-48 (1993)
13. D. M. Shah, and D. L. Anton, Mater. Sci. Engng, **A153**, 402-409 (1992)
14. J. Doychak, J Metals, **44**, 46-51 (1992)
15. C. T. Liu, Sci. of Adv. Mater., (edited by H. Wiedersich and M. Meshii), ASM International, 423-459, (1988)
16. C. T. Liu, and J. O. Stiegler, Sci, **226**, 636-642 (1984)
17. C. T. Liu, C. L. White, and J. A. Horton, Acta Metall., **33**, 213-229 (1985)
18. C. T. Liu, and C. C. Koch, NBSIR-83-2679-2, Washington, D.C. (June 1983)
19. K. Aoki, and O. Izumi, Nippon Kinzoku Gakkaishi, **43** , 1190 (1979)
20. C. T. Liu, C. C. Koch, C. L. White, and E. L. Lee, Proc. Symp. High Temp. Materials Chemistry II, ed. Munir et al., (The Electrochemical Society 1983)
21. C. T. Liu, Structural Intermetallics, (edited by R. Darolia, J. J. Lewandowski, C. T. Liu, P. L. Martin, D. B. Miracle and M.V. Nathal), The Minerals, Metals and Materials Society, 369 (1993)

22. I. Baker, and P. R. Munroe, J Metals, **40**, (1988), 28-31 (1993)

23. W. S. Gibbs, J. J. Petrovic, and R. E. Honnell, Ceram. Eng. Sci. Proc. **8**[7-8], 645-648 (1987)

24. D. H. Carter, J. J. Petrovic, R. E. Honnell, and W. S. Gibbs, Ceram. Eng. Sci. Proc. **10**[9-10], 1121-1129 (1989)

25. M. G. Mendiratta, J. J. Lewandowski, and D.M. Dimiduk, Metall. Trans., **22A**, 1573-1583 (1991)

26. A. K. Gogia, D. Banerjee, and T. K. Nandy, Metall. Trans., **21A**, 609-625 (1990)

27. D. A. Lukasak, and D. A. Koss, Metall. Trans., **21A**, 135-143 (1990)

28. K. Vedula, Strength, JIMIS 6, (edited by O. Izumi), 901-914, (1991)

29. D. H. Carter, and G. F. Hurley, J. Am. Ceram. Soc., **70**, C79-81 (1987)

30. T. C. Lu, A. G. Evans, R. J. Hecht, and R. Mehrabian, Acta Metall Mater. **39**, 1853-1862, (1991)

31. L. Xiano, Y. S. Kim, and R. Abbaschian, Mater. Sci. Engng., **A144**, 277-285 (1991)

32. P. A. Mataga, Acta Metall., **37**, 3349 (1989)

33. J. A. Peters, (ARL/PSU TR 88-088) (July 1988)

34. G. Eriksson, Chemica Scripta 8, 100-103 (1975)

35. M. W. Chase, et. al., JANAF Thermochemical Tables, Third Ed., (Washington, Natl. Bureau of Standards) (1985)

36. Material Safety Data Sheet for SiC whiskers, Advanced Refractory Technologies, 1993

37. R.M. German, "Powder Metallurgy Science", 209 (1984)

38. E.P. Barth and J.K. Tien, Mater. Sci. Engng., **A153**, 398-401 (1992)

39. G. R. Antis, P. Chantikul, B. R. Lawn, and D. B. Marshall., J. Am. Ceram. Soc. **64**, 533-538 (1981)

40. H. Ribes, M. Suery, G. L'Esperance, & J. G. Legoux, Metall. Trans., **21**, 2489-2496 (1990)

41. P.I. Ferreira and R. M. Leal Neto, Intrn. J Powd. Metall., **30**, No. 3, 313-321 (1994)

42. J.C. Murray, R.M. German, Metall. Trans. , **23A**, 2357-2364 (1992)

43. L. Murugesh, K.T. Venkateswara Rao, L.C. DeJonghe and R. O. Ritchie, The Minerals, Metals Society, 65-83 (1991)

44. S. A. Woytera, R. B. Bhagat, and M. F. Amateau, Acta Metall., in press (1995)

APPENDIX A SOLGASMIX Data

Table A3.1. Compounds pertinent to this investigation for use in SOLGASMIX and the availability of free energy data.

Possible Compounds	Initial JANAF Database	Modified Database
Al	x	x
Nb	x	x
Si	x	x
$NbC_{.702}$		x
$NbC_{.98}$	x	x
NbC		x
NbC_2		x
Al_4C_3	x	x
SiC	x	x
NbO	x	x
NbO_2	x	x
Nb_2O_5	x	x
SiO_2	x	x
$NbSi_2$		x
Nb_5Si_3		x
Al_2O_3	x	x
Al_2O_5Si	x	x
$Al_6O_{13}Si_2$	x	x

SOLGASMIX predictions for other system.

Table A3.2 SOLGASMIX predictions for Nb + Si + SiC

Possible Compounds	Molar Amounts	
	Initial	Final
SiC	1.0	0.56
Nb	1.0	0.0
Si	1.0	0.64
NbO_2	0.0	0.0
SiO_2	0.0	0.3
NbO	0.0	0.0
$NbC_{.702}$	0.0	0.09
$NbC_{.98}$	0.0	0.19
NbC	0.0	0.18
$NbSi_2$	0.0	0.34
Nb_5Si_3	0.0	0.04

Table A3.3 SOLGASMIX predictions for Nb + Si + SiO_2 + NbO_2

Possible Compounds	Molar Amounts	
	Initial	Final
SiC	0.0	0.0
Nb	1.0	0.17
Si	1.0	0.0
NbO_2	1.0	0.22
SiO_2	1.0	1.44
NbO	0.0	0.68
$NbC_{.702}$	0.0	0.09
$NbC_{.98}$	0.0	0.19
NbC	0.0	0.18
$NbSi_2$	0.0	0.34
Nb_5Si_3	0.0	0.19

Table A3.4 SOLGASMIX predictions for Mo + Si + SiC

Possible Compounds	Molar Amounts	
	Initial	Final
SiC	1.0	1.0
Mo	1.0	0.0
Si	1.0	0.0
MoO_2	0.0	0.0
SiO_2	0.0	0.0
MoO	0.0	0.0
$MoSi_2$	0.0	0.29
Mo_5Si_3	0.0	0.14

Table A3.5 SOLGASMIX predictions for Mo + Si + SiO_2

Possible Compounds	Molar Amounts	
	Initial	Final
SiC	0.0	0.0
Mo	1.0	0.0
Si	1.0	0.0
Mo_2C	0.0	0.0
MoO_2	0.0	0.0
SiO_2	1.0	1.0
MoO	0.0	0.0
$MoSi_2$	0.0	0.29
Mo_5Si_3	0.0	0.14

Tables A3.6. SOLGASMIX predictions for case 1: Nb + Al + SiC

Possible Compounds	Molar Amounts	
	Initial	Final
Al	1.0	1.0
Nb	1.0	0.0
SiC	1.0	0.3
Si	0.0	0.39
NbC	0.0	0.3
$NbC_{.702}$	0.0	0.16
$NbC_{.98}$	0.0	0.3
$NbSi_2$	0.0	0.13
Nb_5Si_3	0.0	0.02

Table A3.7. SOLGASMIX predictions for case 2: Nb + Al + SiO_2

Possible Compounds	Molar Amounts	
	Initial	Final
Al	1.0	0.05
Nb	1.0	0.33
SiO_2	1.0	0.38
NbO_2	0.0	0.01
NbO	0.0	0.06
Nb_5Si_3	0.0	0.18
Al_2O_5Si	0.0	0.08
Al_2O_3	0.0	0.24

Table A3.8. SOLGASMIX predictions for case 3: Nb + Al + SiO_2 + NbO_2

Possible Compounds	Molar Amounts	
	Initial	Final
Al	1.0	0.14
Nb	1.0	0.27
SiO_2	1.0	0.56
NbO	0.0	0.86
NbO_2	1.0	0.28
Nb_5Si_3	0.0	0.12
Al_2O_5Si	0.0	0.08
Al_2O_3	0.0	0.34

Appendix B TGA Results

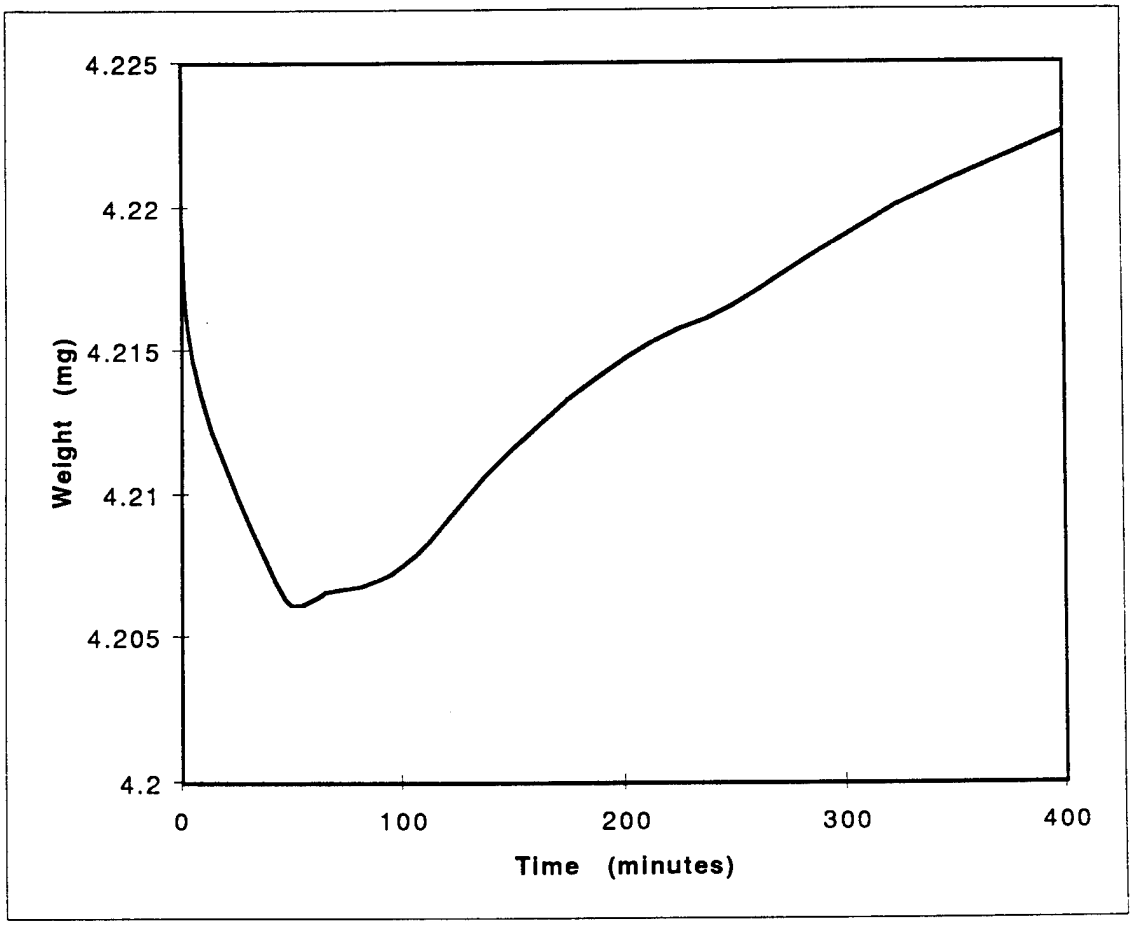

Figure B1. TGA plot for SiC_w at 973 K showing the weight increase (production of oxide layer) vs. time.

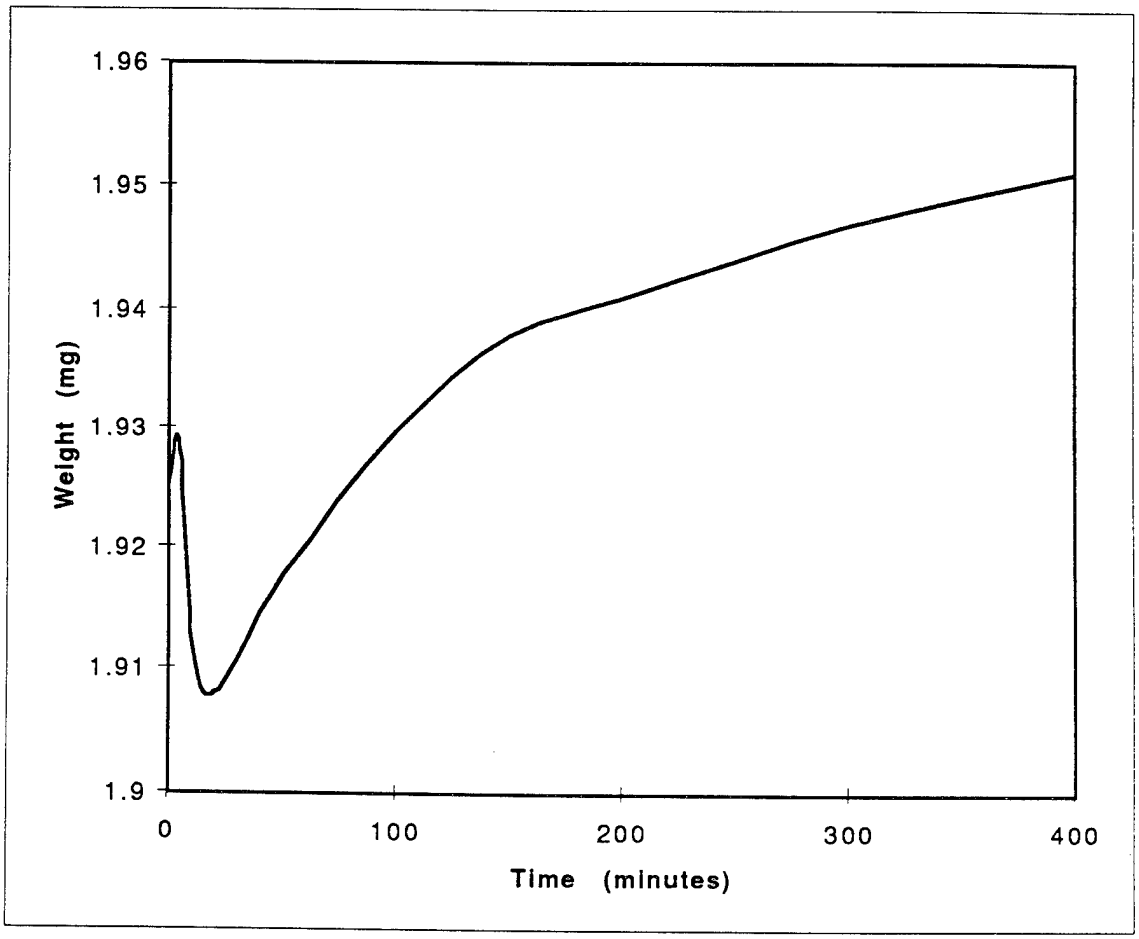

Figure B2. TGA plot for SiC_w at 1073 K showing the weight increase (production of oxide layer) vs. time.

Appendix C

Elemental Mapping of Composite A

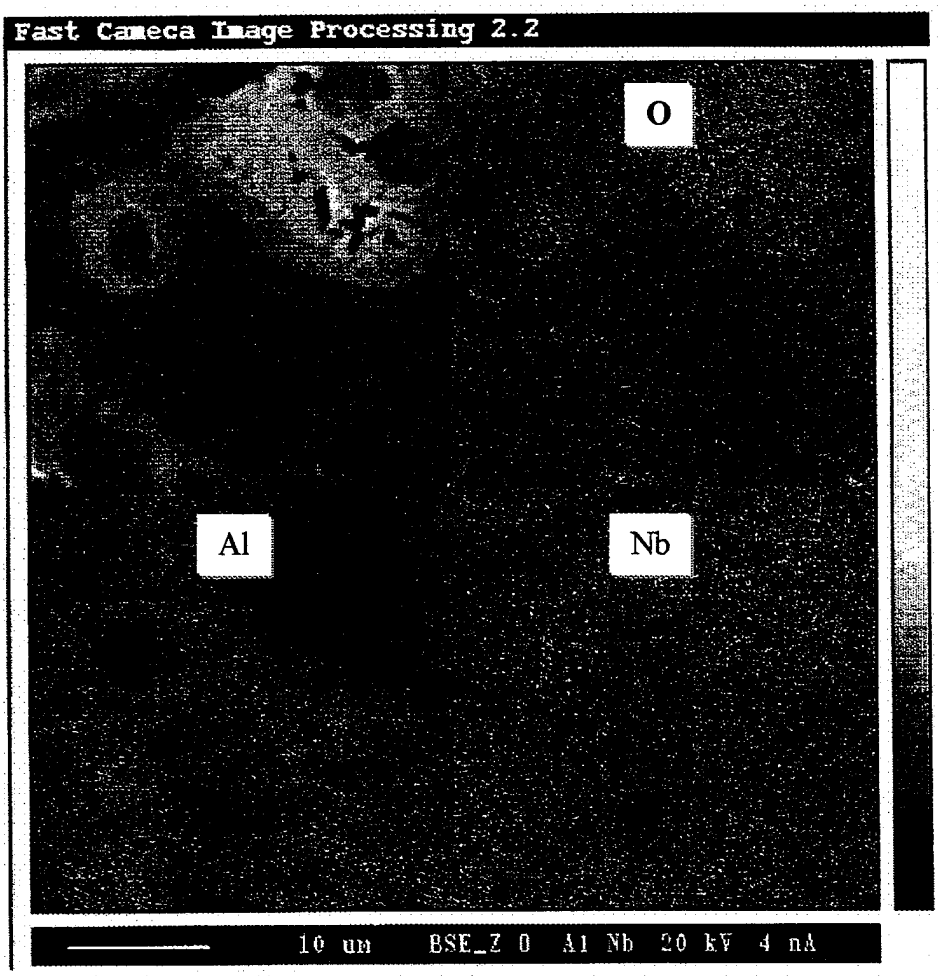

Elemental Mapping of Composite A

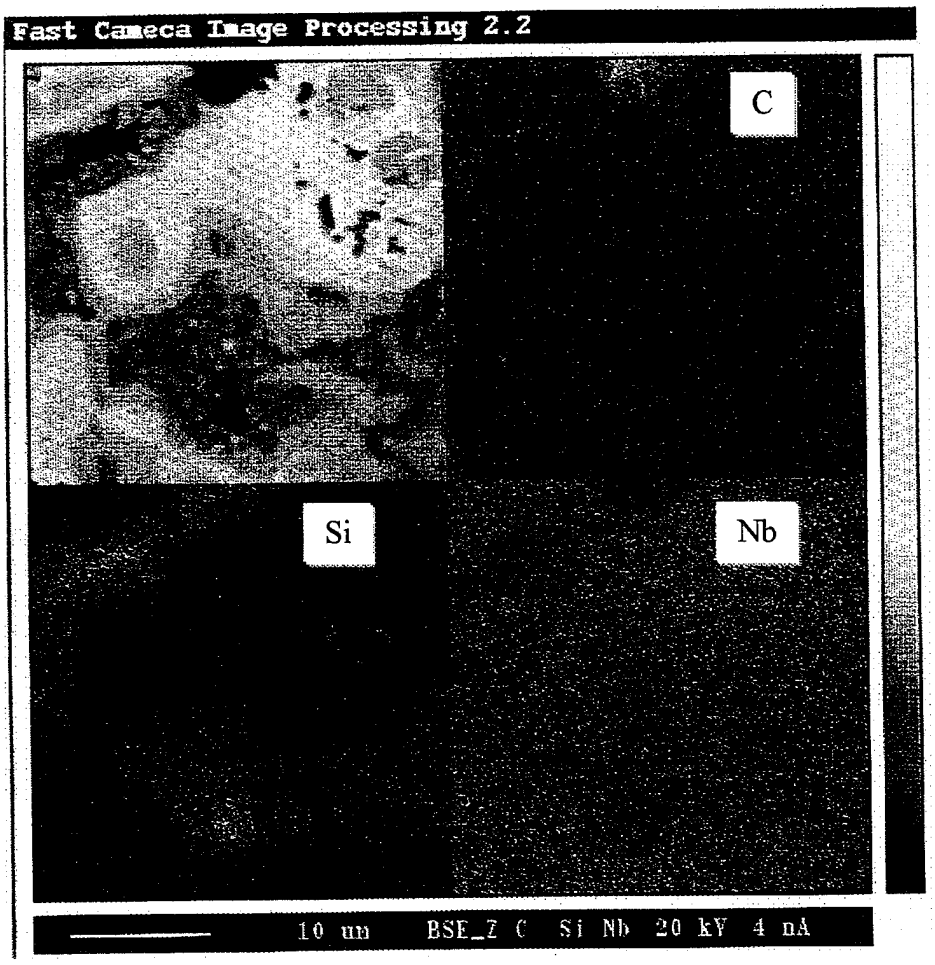

Elemental Mapping of Composite C

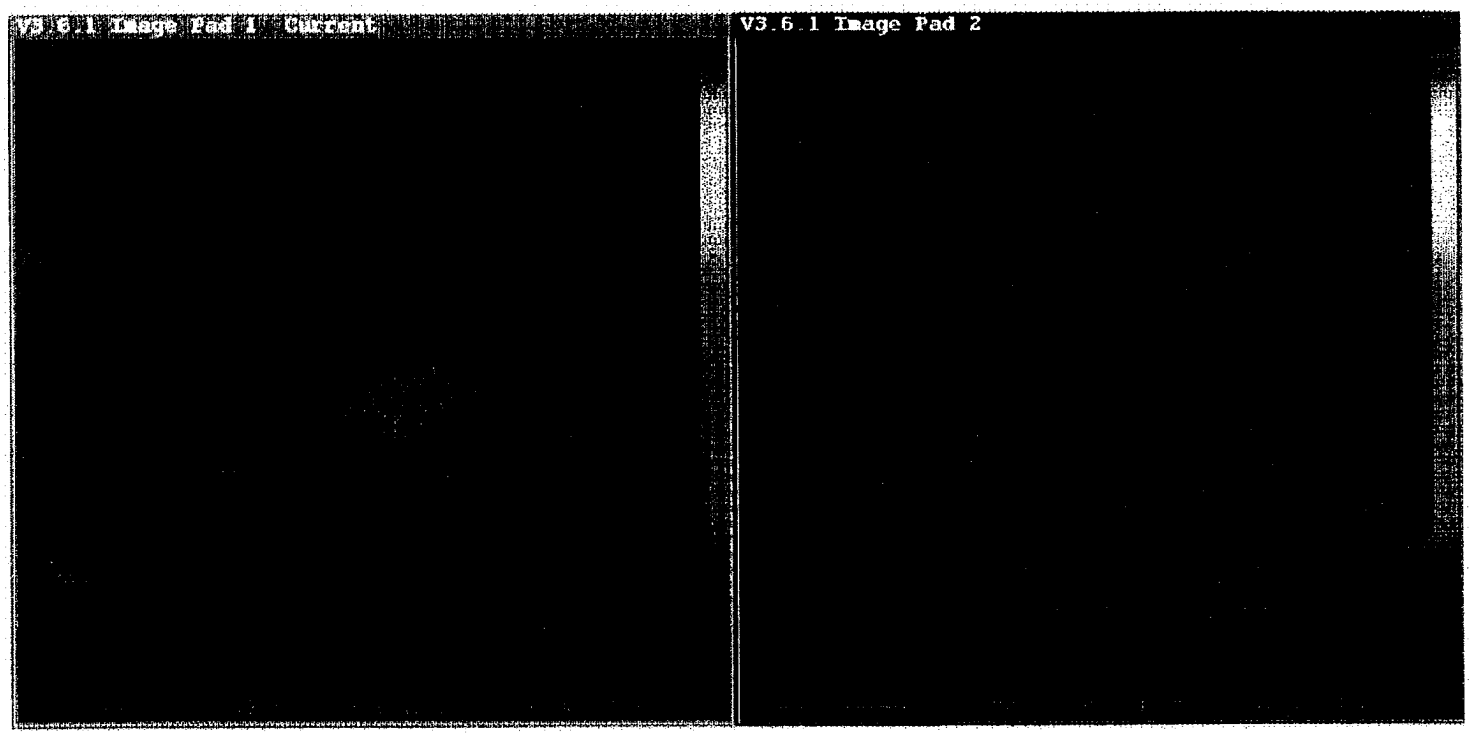

Elemental Mapping of Composite C